CHAPTER II

Capillarity

The topic of capillarity concerns interfaces that are sufficiently mobile to assume an equilibrium shape. The most common examples are meniscuses, thin films, and drops formed by liquids in air or in another liquid. Since it deals with equilibrium configurations, capillarity occupies a place in the general framework of thermodynamics in the context of the macroscopic and statistical behavior of interfaces rather than the details of their molecular structure. In this chapter we describe the measurement of surface tension and present some fundamental results. In Chapter III we discuss the thermodynamics of liquid surfaces.

1. Surface Tension and Surface Free Energy

Although referred to as a *free energy per unit area*, surface tension may equally well be thought of as a force per unit length. Two examples serve to illustrate these viewpoints. Consider, first, a soap film stretched over a wire frame, one end of which is movable (Fig. II-1). Experimentally one observes that a force is acting on the movable member in the direction opposite to that of the arrow in the diagram. If the value of the force per unit length is denoted by γ, then the work done in extending the movable member a distance dx is

$$\text{Work} = \gamma l \, dx = \gamma dA \tag{II-1}$$

where $dA = l\,dx$ is the change in area. In the second formulation, γ appears to be an energy per unit area. Customary units, then, may either be ergs per square centimeter (ergs/cm^2) or dynes per centimeter (dyn/cm); these are identical dimensionally. The corresponding SI units are joules per square meter (J/m^2) or Newtons per meter (N/m); surface tensions reported in dyn/cm and mN/m have the same numerical value.

A second illustration involves the soap bubble. We will choose to think of γ in terms of energy per unit area. In the absence of gravitational or other fields, a soap bubble is spherical, as this is the shape of minimum surface area for an enclosed volume. A soap bubble of radius r has a total surface free energy of $4\pi r^2\gamma$ and, if the radius were to decrease by dr, then the change in surface free energy would be $8\pi r\gamma\, dr$. Since shrinking decreases the surface energy, the tendency to do so must be balanced by a pressure difference across the film

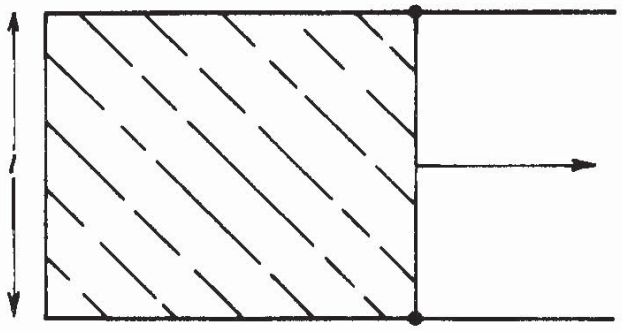

Fig. II-1. A soap film stretched across a wire frame with one movable side.

ΔP such that the work against this pressure difference $\Delta P\, 4\pi r^2\, dr$ is just equal to the decrease in surface free energy. Thus

$$\Delta P\, 4\pi r^2\, dr = 8\pi r\gamma\, dr \tag{II-2}$$

or

$$\Delta P = \frac{2\gamma}{r} \tag{II-3}$$

One thus arrives at the important conclusion that the smaller the bubble, the greater the pressure of the air inside relative to that outside.

The preceding conclusion is easily verified experimentally by arranging two bubbles with a common air connection, as illustrated in Fig. II-2. The arrangement is unstable, and the smaller of the two bubbles will shrink while the other enlarges. Note, however, that the smaller bubble does not shrink indefinitely; once its radius equals that of the tube, its radius of curvature will increase as it continues to shrink until the final stage, where mechanical equilibrium is satisfied, and the two radii of curvature are equal as shown by the dotted lines.

The foregoing examples illustrate the point that equilibrium surfaces may be treated using either the mechanical concept of surface tension or the mathematically equivalent concept of surface free energy. (The derivation of Eq. II-3 from the surface tension point of view is given as an exercise at the end of the chapter). This mathematical equivalence holds everywhere in capillarity phenomena. As discussed in Section III-2, a similar duality of viewpoint can be argued on a molecular scale so that the decision as to whether *surface tension* or *surface free energy* is the more fundamental concept becomes somewhat a matter of individual taste. The term *surface tension* is the older of the two; it goes back to early ideas that the surface of a liquid had some kind of contractile "skin." *Surface free energy* implies only that work is required to bring molecules from the interior of the phase to the surface. Because of its connection to thermodynamic language, these authors consider the latter preferable if

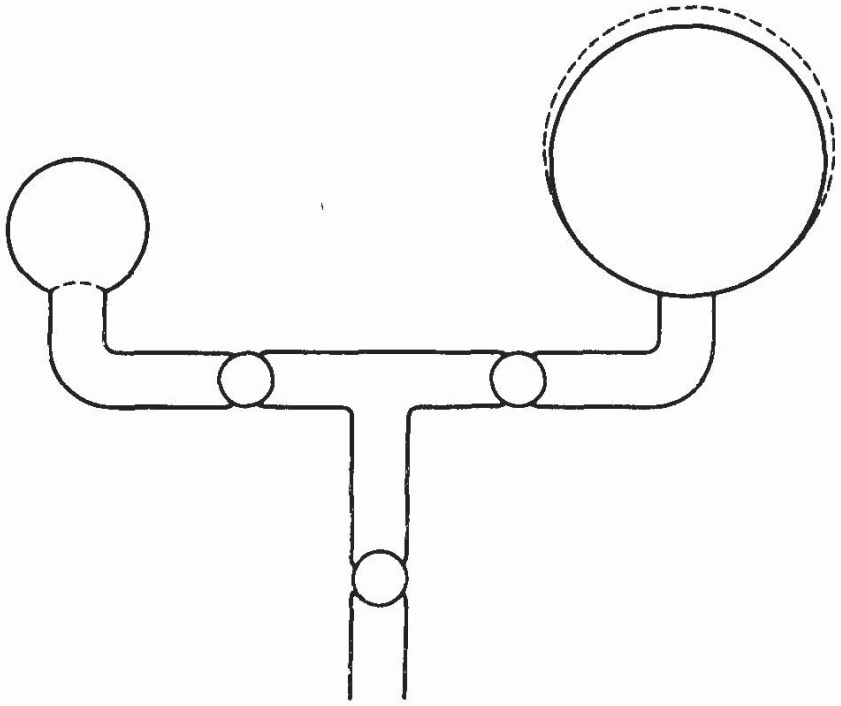

Fig. II-2. Illustration of the Young–Laplace equation.

a choice must be made; however, the two terms are used interchangeably in this book.

2. The Young–Laplace Equation

Equation II-3 is a special case of a more general relationship that is the basic equation of capillarity and was given in 1805 by Young [1] and by Laplace [2]. In general, it is necessary to invoke two radii of curvature to describe a curved surface; these are equal for a sphere, but not necessarily otherwise. A small section of an arbitrarily curved surface is shown in Fig. II-3. The two radii of curvature, R_1 and R_2,† are indicated in the figure, and the section of surface taken

†It is perhaps worthwhile to digress briefly on the subject of radii of curvature. The two radii of curvature for some arbitrarily curved surface are obtained as follows. One defines a normal to the surface at the point in question and then passes a plane through the surface containing the normal. The line of intersection in general will be curved, and the radius of curvature is that for a circle tangent to the line at the point involved. The second radius of curvature is obtained by passing a second plane through the surface, also containing the normal, but perpendicular to the first plane. This gives a second line of intersection and a second radius of curvature.

If the first plane is rotated through a full circle, the first radius of curvature will go through a minimum, and its value at this minimum is called the principal radius of curvature. The second principal radius of curvature is then that in the second plane, kept at right angles to the first. Because Fig. II-3 and Eq. II-7 are obtained by quite arbitrary orientation of the first plane, the radii R_1 and R_2 are not necessarily the principal radii of curvature. The pressure difference ΔP, cannot depend upon the manner in which R_1 and R_2 are chosen, however, and it follows that the sum $(1/R_1 + 1/R_2)$ is independent of how the first plane is oriented (although, of course, the second plane is always at right angles to it).

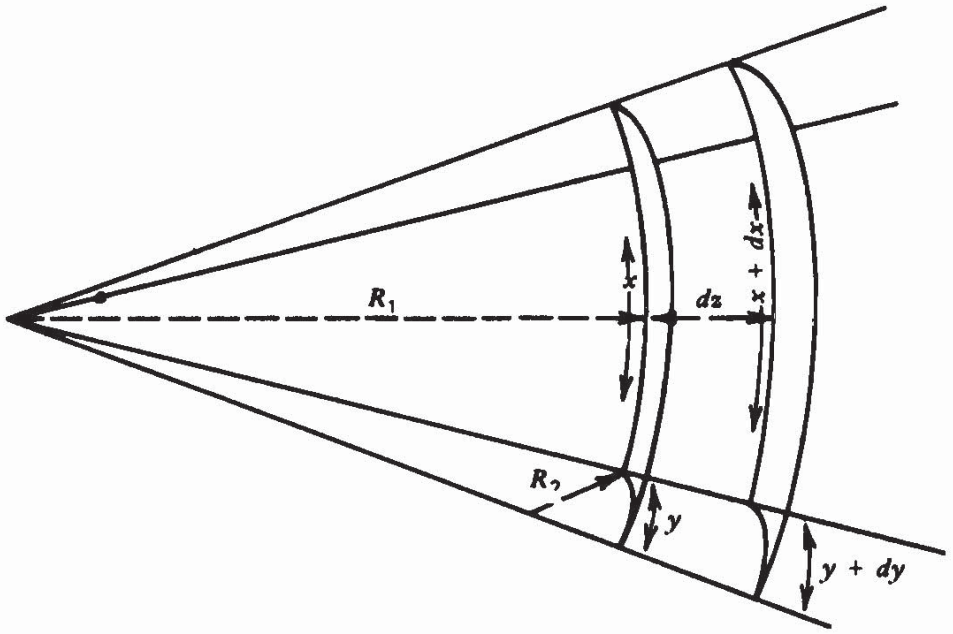

Fig. II-3. Condition for mechanical equilibrium for an arbitrarily curved surface.

is small enough so that R_1 and R_2 are essentially constant. Now if the surface is displaced a small distance outward, the change in area will be

$$\Delta\mathcal{A} = (x + dx)(y + dy) - xy = x\ dy + y\ dx$$

The work done in forming this additional amount of surface is then

$$\text{Work} = \gamma(x\ dy + y\ dx)$$

There will be a pressure difference $\Delta\mathbf{P}$ across the surface; it acts on the area xy and through a distance dz. The corresponding work is thus

$$\text{Work} = \Delta\mathbf{P}\ xy\ dz \tag{II-6}$$

Most of the situations encountered in capillarity involve figures of revolution, and for these it is possible to write down explicit expressions for R_1 and R_2 by choosing plane 1 so that it passes through the axis of revolution. As shown in Fig. II-7*a*, R_1 then swings in the plane of the paper, i.e., it is the curvature of the profile at the point in question. R_1 is therefore given simply by the expression from analytical geometry for the curvature of a line

$$1/R_1 = y''/(1 + y'^2)^{3/2} \tag{II-4}$$

where y' and y'' denote the first and second derivatives with respect to x. The radius R_2 must then be in the plane perpendicular to that of the paper and, for figures of revolution, must be given by extending the normal to the profile until it hits the axis of revolution, again as shown in Fig. II-7*a*. Turning to Fig. II-7*b*, the value of R_2 for the coordinates (x, y) on the profile is given by $1/R_2 = \sin\phi/x$, and since $\tan\phi$ is equal to y', one obtains the following expression for R_2:

$$1/R_2 = y'/x(1 + y'^2)^{1/2} \tag{II-5}$$

From a comparison of similar triangles, it follows that

$$\frac{x + dx}{R_1 + dz} = \frac{x}{R_1} \text{ or } dx = \frac{x\, dz}{R_1}$$

and

$$\frac{y + dy}{R_2 + dz} = \frac{y}{R_2} \text{ or } dy = \frac{y\, dz}{R_2}$$

If the surface is to be in mechanical equilibrium, the two work terms as given must be equal, and on equating them and substituting in the expressions for dx and dy, the final result obtained is

$$\Delta \mathbf{P} = \gamma \left(\frac{1}{R_1} + \frac{1}{R_2} \right) \tag{II-7}$$

Equation II-7 is the fundamental equation of capillarity and will recur many times in this chapter.

It is apparent that Eq. II-7 reduces to Eq. II-3 for the case of both radii being equal, as is true for a sphere. For a plane surface, the two radii are each infinite and $\Delta \mathbf{P}$ is therefore zero; thus there is no pressure difference across a plane surface.

3. Some Experiments with Soap Films

There are a number of relatively simple experiments with soap films that illustrate beautifully some of the implications of the Young–Laplace equation. Two of these have already been mentioned. Neglecting gravitational effects, a film stretched across a frame as in Fig. II-1 will be planar because the pressure is the same as both sides of the film. The experiment depicted in Fig. II-2 illustrates the relation between the pressure inside a spherical soap bubble and its radius of curvature; by attaching a manometer, $\Delta \mathbf{P}$ could be measured directly.

An interesting set of shapes results if one forms a soap bubble or liquid bridge between two cylindrical supports, as shown in Fig. II-4. In Fig. II-4*a*, the upper support is open to the atmosphere so that the pressure is everywhere the same, and ΔP must be zero. Although the surface appears to be curved, Eq. II-7 is not contradicted. The two radii of curvature indicated in Fig. II-4*a*, where R_1 swings in the plane of the paper and R_2 swings in the plane perpendicular to it, are equal in magnitude and opposite in sign because they originate on opposite sides of the film; hence they cancel each other in Eq. II-7. This is an example of a surface with zero mean curvature. Such surfaces are found in other situations such as static "dewetting holes" (see Chapter XIII).

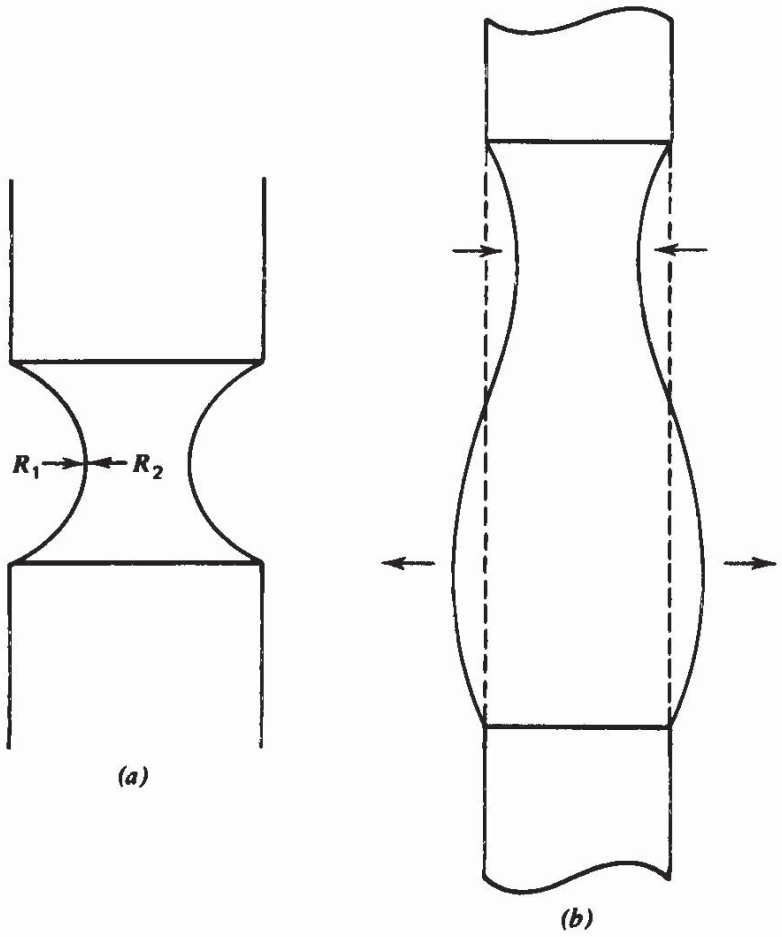

Fig. II-4. (*a*) A cylindrical soap film; (*b*) manner of a collapse of a cylindrical soap film of excessive length.

Instability of Cylindrical Columns. C. V. Boys, in his elegant little monograph of 1890 [3], discusses an important property of quasistatic cylindrical films that was first studied in cylindrical columns of fluids by Lord Rayleigh in 1879. If the soap film in Fig. II-4*a* were made to be cylindrical by adjusting the gas pressure inside, it, like a cylindrical thread of fluid, would be unstable to surface waves whose length exceeds the circumference of the cylinder. The column would contract at one end and bulge at the other, as illustrated in Fig. II-4*b*, before breaking up into a smaller and larger bubble (or drop) as shown in the photographs of a liquid stream in Fig. II-5 [4]. The mechanism is associated with the nonzero curvature of the static state and the fact that fluctuations establish capillary pressure gradients that drive the fluid away from the equilibrium. It is now recognized that capillary breakup is a particularly simple example of the geometric instability of states of static equilibrium in the presence of surface tension. For a general description dealing with pendant and sessile drops, finite cylinders (capillary bridges) and other capillary surfaces, see Michael [5]. A detailed discussion of the capillary break up of jets, including several interesting practical applications, is given by Bogy [6]. The case of one liquid in a second, immiscible one is discussed in Refs. 6a and 7. A similar instability occurring in a thin annular coating inside a capillary can have important consequences for capillary columns in chromatography [8].

Returning to equilibrium shapes, these have been determined both experimentally and by solution of the Young–Laplace equation for a variety of situations. Examples

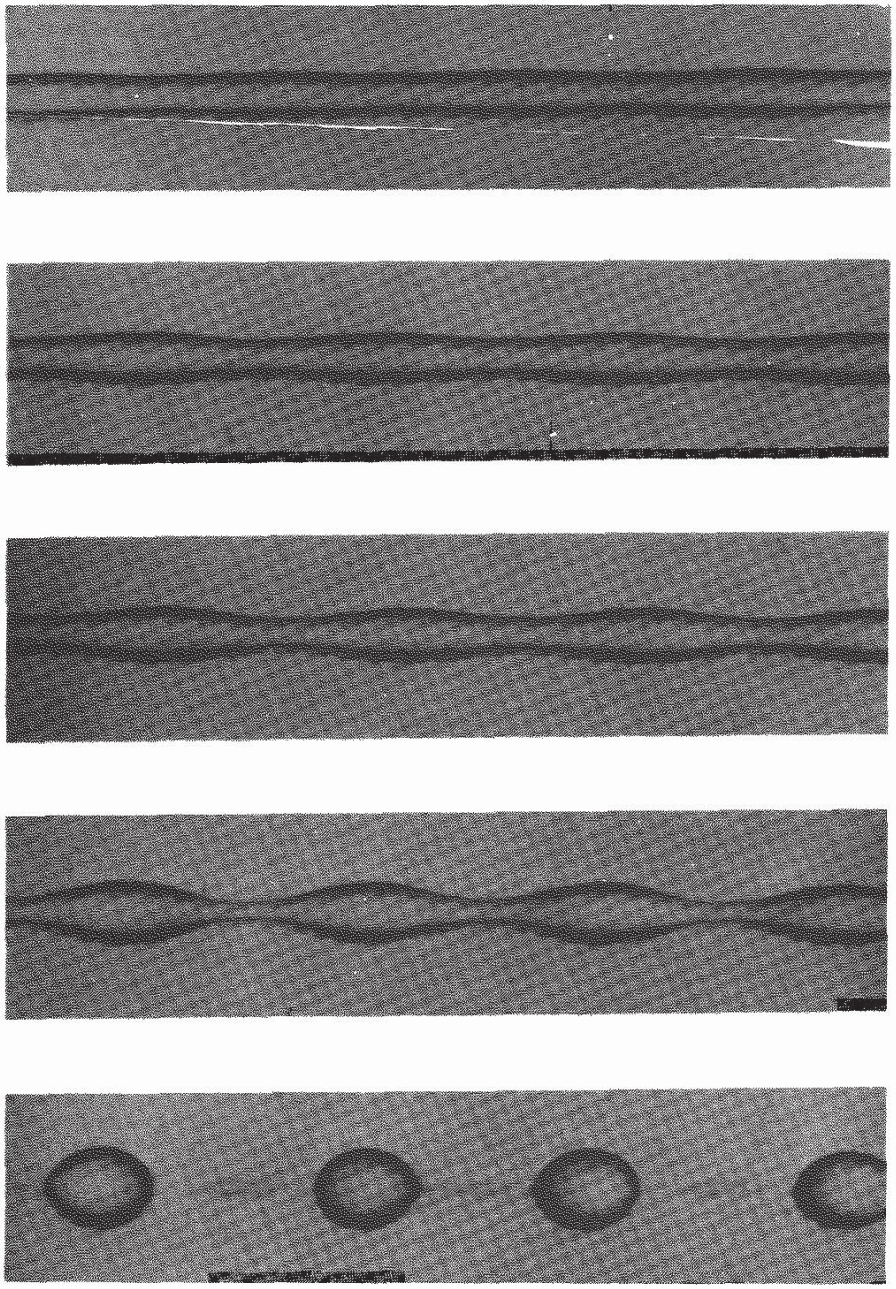

Fig. II-5. Necking in a liquid stream. [Courtesy S. G. Mason (4).]

include the shape of a liquid plug in capillary tubes of various shapes of cross sections (9) and of liquid bridges between spheres in a gravitational field [10]; see Refs. 11 to 12 for reviews.

4. The Treatment of Capillary Rise

A. Introductory Discussion

An approximate treatment of the phenomenon of capillary rise is easily made in terms of the Young–Laplace equation. If the liquid completely wets the wall of the capillary, the liquids surface is thereby constrained to lie parallel to the wall at the region of contact and the surface must be concave in shape. The

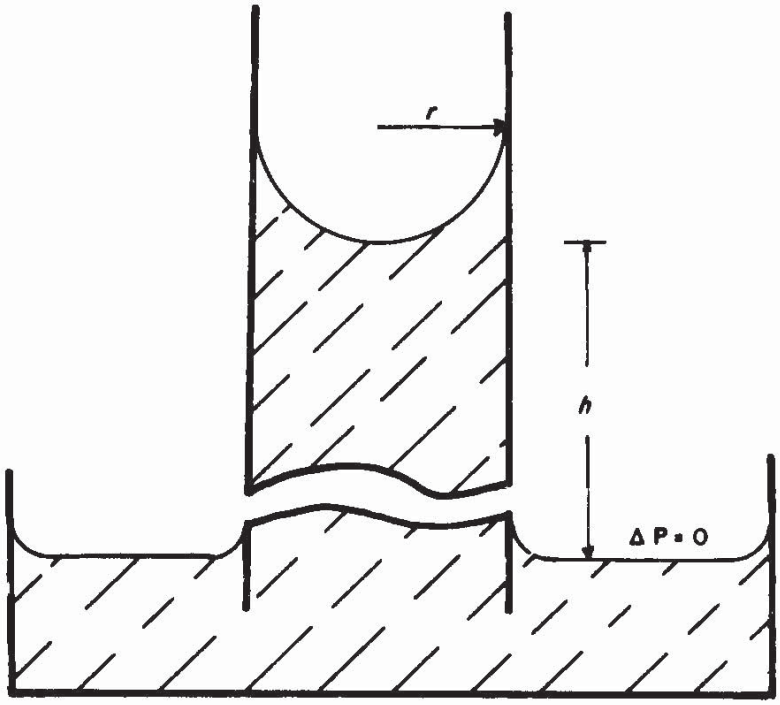

Fig. II-6. Capillary rise (capillary much magnified in relation to dish).

radii of curvature are defined in terms of an outward normal from the liquid; thus, it follows from Eq. II-7 that the pressure is lower in the liquid than in the gas phase. Small circular capillaries will have an approximately hemispherical meniscus as illustrated in Fig. II-6. Here the two radii of curvature are equal to each other and to the radius of the capillary. Eq. II-7 then reduces to

$$\Delta \mathbf{P} = \frac{2\gamma}{r} \tag{II-8}$$

where r is the radius of the capillary. If h denotes the height of the meniscus above a *flat* liquid surface (for which $\Delta \mathbf{P}$ must be zero), then $\Delta \mathbf{P}$ in Eq. II-8 must also equal the hydrostatic pressure drop in the column of liquid in the capillary. Thus $\Delta \mathbf{P} = \Delta\rho\, gh$, where $\Delta\rho$ denotes the difference in density between the liquid and gas phases and g is the acceleration due to gravity. Equation II-8 becomes

$$\Delta\rho\, gh = \frac{2\gamma}{r} \tag{II-9}$$

or

$$a^2 = \frac{2\gamma}{\Delta\rho\, g} = rh \tag{II-10}$$

The quantity a, defined by Eq. II-10 is known as the *capillary constant* or *cap-*

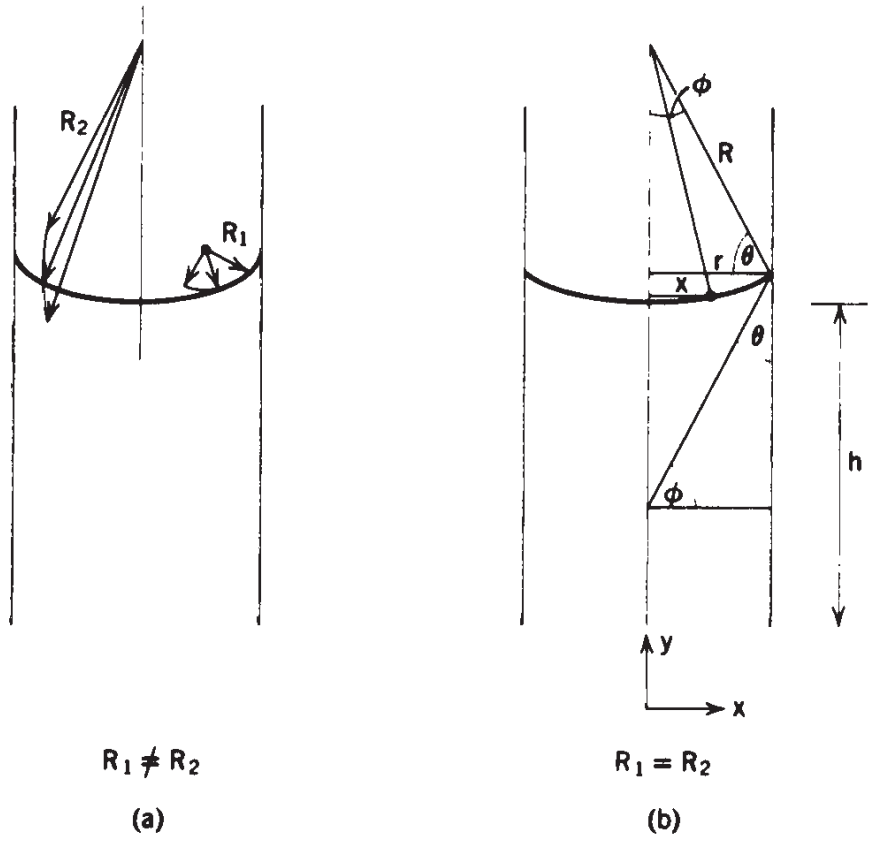

Fig. II-7. The meniscus in a capillary as a figure of revolution.

illary length. The factor of 2 in the definition of a arises from this particular boundary value problem; for many other situations the capillary length is defined by $a^2 = \gamma/\Delta\rho g$ (see Section X-6A).

Similarly, the identical expression holds for a liquid that completely fails to wet the capillary walls, where there will be an angle of contact between the liquid and the wall of 180°, a convex meniscus and a capillary depression of depth h.

A slightly more general case is that in which the liquid meets the circularly cylindrical capillary wall at some angle θ, as illustrated in Fig. II-7. If the meniscus is still taken to be spherical in shape, it follows from simple geometric consideration that $R_2 = r/\cos\theta$ and, since $R_1 = R_2$, Eq. II-9 then becomes

$$\Delta\rho\, gh = \frac{2\gamma\cos\theta}{r} \tag{II-11}$$

B. Exact Solutions to the Capillary Rise Problem

The exact treatment of capillary rise must take into account the deviation of the meniscus from sphericity, that is, the curvature must correspond to the $\Delta P = \Delta\rho\, gy$ at each point on the meniscus, where y is the elevation of that point above the flat liquid surface. The formal statement of the condition is obtained by writing the Young–Laplace equation for a general point (x, y) on the meniscus, with R_1 and R_2 replaced by the expressions from analytical geometry given in

the footnote to Section II-2. We still assume that the capillary is circular in cross section so that the meniscus shape is that of a figure of revolution; as indicated in Fig. II-7, R_1 swings in the plane of paper, and R_2 in the plane perpendicular to the paper. One thus obtains

$$\Delta\rho\, gy = \gamma\left[\frac{y''}{(1+y'^2)^{3/2}} + \frac{y'}{x(1+y'^2)^{1/2}}\right] \tag{II-12}$$

where $y' = dy/dx$ and $y'' = d^2y/dx^2$, as in Eqs. II-4 and II-5. A compact alternative form is

$$\bar{y} = \frac{1}{\bar{x}}\,\frac{d}{d\bar{x}}\,(\bar{x}\sin\phi) \tag{II-13}$$

where a bar denotes that the quantity has been made dimensionless by multiplication by $\sqrt{2/a}$ (see Refs. 10 and 13).

Equations II-12 and II-13 illustrate that the shape of a liquid surface obeying the Young–Laplace equation with a body force is governed by *differential equations* requiring boundary conditions. It is through these boundary conditions describing the interaction between the liquid and solid wall that the contact angle enters.

The total weight of the column of liquid in the capillary follows from Eq. II-12:

$$W = 2\pi r\gamma\cos\theta \tag{II-14}$$

This is *exact*—see Problem II-8. Notice that Eq. II-14 is exactly what one would write, assuming the meniscus to be "hanging" from the wall of the capillary and its weight to be supported by the vertical component of the surface tension, $\gamma\cos\theta$, multiplied by the circumference of the capillary cross section, $2\pi r$. Thus, once again, the mathematical identity of the concepts of *surface tension* and *surface free energy* is observed.

While Eq. II-14 is exact, its use to determine surface tension from capillary rise experiments is not convenient. More commonly, one measures the height, h, to the *bottom* of the meniscus.

Approximate solutions to Eq. II-12 have been obtained in two forms. The first, given by Lord Rayleigh [13], is that of a series approximation. The derivation is not repeated here, but for the case of a nearly spherical meniscus, that is, $r \ll h$, expansion around a deviation function led to the equation

$$a^2 = r\left(h + \frac{r}{3} - \frac{0.1288r^2}{h} + \frac{0.1312r^3}{h^2} \cdots\right) \tag{II-15}$$

The first term gives the elementary equation (Eq. II-10). The second term takes into account the weight of the meniscus, assuming it to be spherical (see Problem II-3). The succeeding terms provide corrections for deviation from sphericity.

The general case has been solved by Bashforth and Adams [14], using an iterative method, and extended by Sugden [15], Lane [16], and Paddy [17]. See also Refs. 11 and 12. In the case of a figure of revolution, the two radii of curvature must be equal at the apex (i.e., at the bottom of the meniscus in the case of capillary rise). If this radius of curvature is denoted by b, and the elevation of a general point on the surface is denoted by z, where $z = y - h$, then Eq. II-7 can be written

$$\gamma\left(\frac{1}{R_1}+\frac{1}{R_2}\right)=\Delta\rho\, gz+\frac{2\gamma}{b} \tag{II-16}$$

Thus, at $z = 0$, $\Delta\mathbf{P} = 2\gamma/b$, and at any other value of z, the change in $\Delta\mathbf{P}$ is given by $\Delta\rho\, gz$. Equation II-16 may be rearranged so as to involve only dimensionless parameters

$$\frac{1}{R_1/b}+\frac{\sin\phi}{x/b}=\beta\,\frac{z}{b}+2 \tag{II-17}$$

where R_2 has been replaced by its equivalent, $x/\sin\phi$, and the dimensionless quantity β is referred to as the Bond number, given by

$$\beta=\frac{\Delta\rho g b^2}{\gamma}=\frac{2b^2}{a^2} \tag{II-18}$$

where small Bond numbers indicate weak body forces or strong surface tensions. This parameter is positive for oblate figures of revolution, that is, for a sessile drop, a bubble under a plate, and a meniscus in a capillary. It is negative for prolate figures, that is, for a pendant drop or a clinging bubble.

Bashforth and Adams obtained solutions to Eq. II-17 (with R_1 replaced by the expression in analytical geometry), using a numerical integration procedure (this was before the day of high-speed digital computers, and their work required tremendous labor). Their results are reported as tables of values of x/b and z/b for closely spaced values of β and of ϕ. For a given β value, a plot of z/b versus x/b gives the profile of a particular figure of revolution satisfying Eq. II-17. By way of illustration, their results for $\beta = 80$ are reproduced (in abbreviated form) in Table II-1. Observe that x/b reaches a maximum at $\phi = 90°$, so that in the case of zero contact angle the surface is now tangent to the capillary wall and hence $(x/b)_{max} = r/b$. The corresponding value of r/a is given by $(r/b)\sqrt{\beta/2}$. In this manner, Sugden compiled tables of r/b versus r/a.

TABLE II-1
Solution to Eq. II-17 for $\beta = 80$

ϕ (deg)	x/b	z/b	ϕ (deg)	x/b	z/b
5	0.08159	0.00345	100	0.33889	0.17458
10	0.14253	0.01133	110	0.33559	0.18696
20	0.21826	0.03097	120	0.33058	0.19773
30	0.26318	0.05162	130	0.32421	0.20684
40	0.29260	0.07204	140	0.31682	0.21424
50	0.31251	0.09183	150	0.30868	0.21995
60	0.32584	0.11076	160	0.30009	0.22396
70	0.33422	0.12863	170	0.29130	0.22632
80	0.33872	0.14531			
90	0.34009	0.16067			

Lane improved on these tables with accurate polynomial fits to numerical solutions of Eq. II-17 [16]. Two equations result; the first is applicable when $r/a \leq 2$

$$b/r = 1 + [3327.9(r/a)^2 + 65.263(r/a)^3 - 473.926(r/a)^4 + 663.569(r/a)^5 - 300.032(r/a)^6 + 75.1929(r/a)^7 - 7.3163(r/a)^8]/10^4 \qquad \text{(II-19)}$$

and another is to be employed when $r/a \geq 2$

$$r/b = (r/a)^{3/2} \exp[-1.41222(r/a) + 0.66161 + 0.14681(a/r) + 0.37136(a/r)^2] \qquad \text{(II-20)}$$

The use of these equations is perhaps best illustrated by means of a numerical example. In a measurement of the surface tension of benzene, the following data are obtained:

Capillary radius—0.0550 cm

Density of benzene—0.8785; density of air—0.0014 (both at 20°C);

hence $\Delta\rho = 0.8771$ g/ml

Height of capillary rise—1.201 cm

We compute a first approximation to the value of the capillary constant a_1 by means of Eq. II-10 ($a^2 = rh$). The ratio r/a_1 is then obtained and the corresponding value of r/b is determined from Eq. II-19 or II-20; in the present case, $a_1^2 = 1.201 \times 0.0550 = 0.660$; hence, $r/a_1 = 0.0550/0.2570 = 0.2140$. From Eq. II-19, r/b_1 is then 0.9850. Since b is the value of R_1 and of R_2 at the bottom of the meniscus, the equation $a^2 = bh$ is exact. From the value of r/b_1, we obtain a first approximation to b, that is, $b_1 = 0.0550/0.9850 = 0.05584$. This value of b gives a second approximation to a from $a_2^2 = b_1 h = 0.05584 \times 1.201 = 0.06706$. A second round of approximations is not needed in this case but would be carried out by computing r/a_2; then from Eq. II-19, r/b_2, and

so on. The value of 0.06706 for a_2^2 obtained here leads to 28.84 dyn/cm for the surface tension of benzene (at 20°).

The calculation may be repeated in SI units (see, however, Ref. 18). The radius is now 5.50×10^{-4} m, the densities become 878.5 and 1.4 kg/m^3, and h is 1.20×10^{-2} m. We find $a_1^2 = 6.60 \times 10^{-6}$ m^2; the dimensionless ratio r/a_1 remains unchanged. The final approximation gives $a_1^2 = 6.706 \times 10^{-6}$ m^2, whence

$$\gamma = \frac{877.1 \times 9.807 \times 6.706 \times 10^{-6}}{2} = 2.884 \times 10^{-2} \text{N/m(or J/m}^2\text{)} \qquad \text{(II-21)}$$

This answer could have been stated as 28.84 mN/m (or dyn/cm).

C. Experimental Aspects of the Capillary Rise Method

The capillary rise method is generally considered to be the most accurate means to measure γ, partly because the theory has been worked out with considerable exactitude and partly because the experimental variables can be closely controlled. This is to some extent a historical accident, and other methods now rival or surpass the capillary rise one in value.

Perhaps the best discussions of the experimental aspects of the capillary rise method are still those given by Richards and Carver [20] and Harkins and Brown [21]. *For the most accurate work, it is necessary that the liquid wet the wall of the capillary so that there be no uncertainty as to the contact angle.* Because of its transparency and because it is wet by most liquids, a glass capillary is most commonly used. The glass must be very clean, and even so it is wise to use a receding meniscus. The capillary must be accurately vertical, of accurately known and uniform radius, and should not deviate from circularity in cross section by more than a few percent.

As is evident from the theory of the method, h must be the height of rise above a surface for which ΔP is zero, that is, a flat liquid surface. In practice, then, h is measured relative to the surface of the liquid in a wide outer tube or dish, as illustrated in Fig. II-6, and it is important to realize that there may not be an appreciable capillary rise in relatively wide tubes. Thus, for water, the rise is 0.04 mm in a tube 1.6 cm in radius, although it is only 0.0009 mm in one of 2.7-cm radius.

The general attributes of the capillary rise method may be summarized as follows. It is considered to be one of the best and most accurate absolute methods, good to a few hundredths of a percent in precision. On the other hand, for practical reasons, a zero contact angle is required, and fairly large volumes of solution are needed. With glass capillaries, there are limitations as to the alkalinity of the solution. For variations in the capillary rise method, see Refs. 11, 12, and 22–26.

5. The Maximum Bubble Pressure Method

The procedure, as indicated in Fig. II-8, is to slowly blow bubbles of an inert gas in the liquid in question by means of a tube projecting below the surface. As also illustrated in the figure, for *small* tubes, the sequence of shapes assumed by the bubble during its growth is such that, while it is always a section of a sphere, its radius goes through a minimum when it is just hemispherical. At this point the radius is equal to that of the tube and, since the radius is at a minimum, ΔP is at a maximum. The value of ΔP is then given by Eq. II-3, where r is the radius of the tube. If the liquid wets the material of the tube, the bubble will form from the inner wall, and r will then be the inner radius of the tube. Experimentally, then, one measures the maximum gas pressure in the tube such that bubbles are unable to grow and break away. Referring again to Fig. II-8, since the tube is some arbitrary distance t below the surface of the liquid, ΔP_{max} is given by $(P_{max} - P_t)$, where P_{max} is the measured maximum pressure and P_t is the pressure corresponding to the hydrostatic head t.

If ΔP_{max} is expressed in terms of the corresponding height of a column of the liquid, that is, $\Delta P_{max} = \Delta\rho\, gh$, then the relationship becomes identical to that for the simple capillary rise situation as given by Eq. II-10.

It is important to realize that the preceding treatment is the limiting one for sufficiently small tubes and that significant departures from the limiting Eq. II-10 occur for r/a values as small as 0.05. More realistically, the situation is as shown in Fig. II-9, and the maximum pressure may not be reached until ϕ is considerably greater than 90°.

As in the case of capillary rise, Sugden [27] has made use of Bashforth's and Adams' tables to calculate correction factors for this method. Because the figure is again one of revolution, the equation $h = a^2/b + z$ is exact, where b is the value of $R_1 = R_2$ at the origin and z is the distance of OC. The equation simply states that ΔP, expressed as height of a column of liquid, equals the sum of the hydrostatic head and the pressure

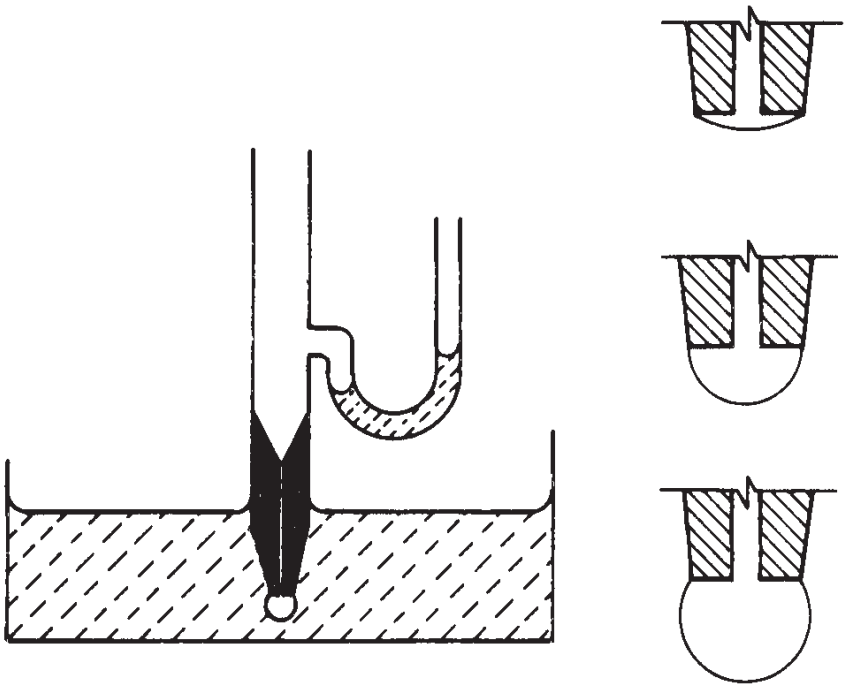

Fig. II-8. Maximum bubble pressure method.

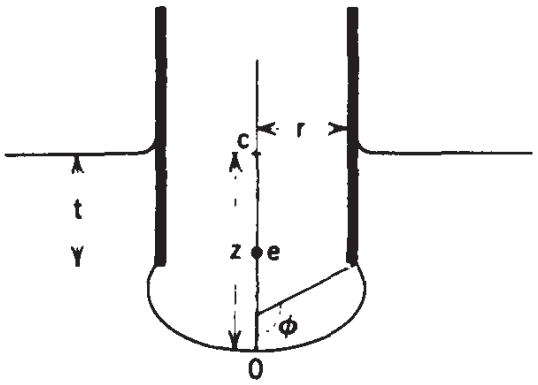

Fig. II-9

change across the interface; by simple manipulation, it may be put in the form

$$\frac{r}{X} = \frac{r}{b} + \frac{r}{a}\,\frac{z}{b}\left(\frac{\beta}{2}\right)^{1/2} \tag{II-22}$$

where β is given by Eq. II-18 and $X = a^2/h$. For any given value of r/a there will be a series of values of r/X corresponding to a series of values of β and of ϕ. For each assumed value of r/a, Sugden computed a series of values of r/b by inserting various values of β in the identity $r/b = (r/a)(2/\beta)^{1/2}$. By means of the Bashforth and Adams tables [14], for each β value used and corresponding r/b value, a value of z/b and hence of r/X (by Eq. II-22) was obtained. Since r/X is proportional to the pressure in the bubble, the series of values for a given r/a go through a maximum as β is varied. For each assumed value, Sugden then tabulated this maximum value of r/X. His values are given in Table II-2 as X/r versus r/a

The table is used in much the same manner as are Eqs. II-19 and II-20 in the case of capillary rise. As a first approximation, one assumes the simple Eq. II-10 to apply, that is, that $X = r$; this gives the first approximation a_1 to the capillary constant. From this, one obtains r/a_1 and reads the corresponding value of X/r from Table II-2. From the derivation of $X(X = a^2/h)$, a second approximation a_2 to the capillary constant is obtained, and so on. Some more recent calculations have been made by Johnson and Lane [28].

The maximum bubble pressure method is good to a few tenths percent accuracy, does not depend on contact angle (except insofar as to whether the inner or outer radius of the tube is to be used), and requires only an approximate knowledge of the density of the liquid (if twin tubes are used), and the measurements can be made rapidly. The method is also amenable to remote operation and can be used to measure surface tensions of not easily accessible liquids such as molten metals [29].

A pulsating bubble surfactometer, available commercially, allows one to measure the dynamic surface tension in solutions [30, 31]. The bubble is expanded and contracted to change its area by a factor of 1.5–2 at rates of 1–100 cycles per minute. Studying hexadecanol in water, an important component of a lung surfactant replacement drug, Franses and co-workers [30] illustrate the importance of the geometry of the measuring technique in the study of surfactant dispersions. In the pulsating bubble technique, hexadecanol particles rise to the surface enhancing flux and speeding the reduction in

TABLE II-2
Correction Factors for the Maximum Bubble Pressure Method (Minimum Values of X/r for Values of r/a from 0 to 1.50)

r/a	0.00	0.01	0.02	0.03	0.04	0.05	0.06	0.07	0.08	0.09
0.0	1.0000	9999	9997	9994	9990	9984	9977	9968	9958	9946
0.1	0.9934	9920	9905	9888	9870	9851	9831	9809	9786	9762
0.2	9737	9710	9682	9653	9623	9592	9560	9527	9492	9456
0.3	9419	9382	9344	9305	9265	9224	9182	9138	9093	9047
0.4	9000	8952	8903	8853	8802	8750	8698	8645	8592	8538
0.5	8484	8429	8374	8319	8263	8207	8151	8094	8037	7979
0.6	7920	7860	7800	7739	7678	7616	7554	7493	7432	7372
0.7	7312	7252	7192	7132	7072	7012	6953	6894	6835	6776
0.8	6718	6660	6603	6547	6492	6438	6385	6333	6281	6230
0.9	6179	6129	6079	6030	5981	5933	5885	5838	5792	5747
1.0	5703	5659	5616	5573	5531	5489	5448	5408	5368	5329
1.1	5290	5251	5213	5176	5139	5103	5067	5032	4997	4962
1.2	4928	4895	4862	4829	4797	4765	4733	4702	4671	4641
1.3	4611	4582	4553	4524	4496	4468	4440	4413	4386	4359
1.4	4333	4307	4281	4256	4231	4206	4181	4157	4133	4109
1.5	4085									

surface tension; in the pendant drop technique (see Section II-7A) the buoyant particles are depleted at the interface.

6. Detachment Methods

Several convenient ways to measure surface tension involve the detachment of a solid from the liquid surface. These include the measurement of the weight in a drop falling from a capillary and the force to detach a ring, wire, or thin plate from the surface of a liquid. In this section we briefly describe these methods and their use.

A. The Drop Weight Method

This is a fairly accurate and convenient method for measuring the surface tension of a liquid–vapor or liquid–liquid interface. The procedure, in its simplest form, is to form drops of the liquid at the end of a tube, allowing them to fall into a container until enough have been collected to accurately determine the weight per drop. Recently developed computer-controlled devices track individual drop volumes to $\pm = 0.1$ μl [32].

The method is a very old one, remarks on it having been made by Tate in 1864 (33), and a simple expression for the weight W of a drop is given by what

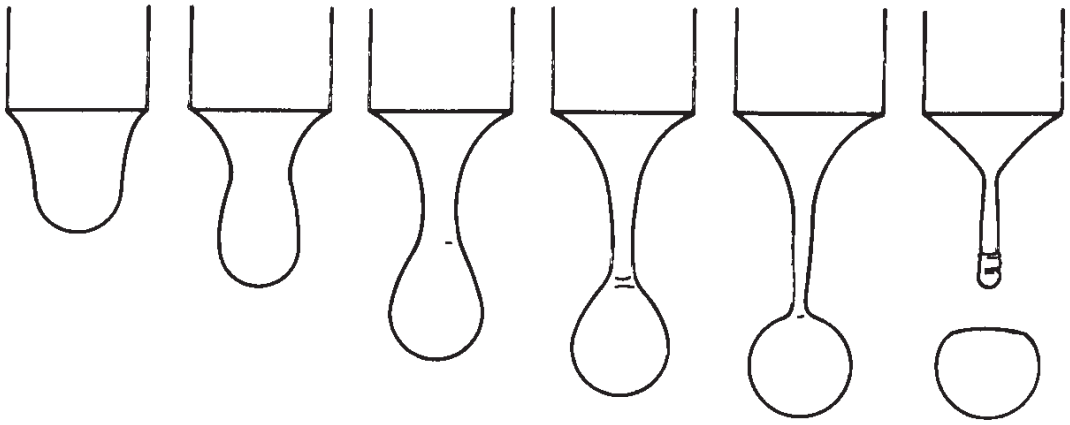

Fig. II-10. High-speed photographs of a falling drop.

is known as *Tate's law*† :

$$W = 2\pi r\gamma \tag{II-22}$$

Here again, the older concept of "surface tension" appears since Eq. II-22 is best understood in terms of the argument that the maximum force available to support the weight of the drop is given by the surface tension force per centimeter times the circumference of the tip.

In actual practice, a weight W' is obtained, which is less than the "ideal" value W. The reason for this becomes evident when the process of drop formation is observed closely. What actually happens is illustrated in Fig. II-10. The small drops arise from the mechanical instability of the thin cylindrical neck that develops (see Section II-3); in any event, it is clear that only a portion of the drop that has reached the point of instability actually falls—as much as 40% of the liquid may remain attached to the tip.

The usual procedure is to apply a correction factor f to Eq. II-22, so that W' is given by

$$W' = 2\pi r\gamma f$$

Harkins and Brown [21] concluded that f should be a function of the dimensionless ratio r/a or, alternatively, of $r/V^{1/3}$, where V is the drop volume. (See Refs. 34 and 35 for a more up-to-date discussion.) This they verified experimentally by determining drop weights for water and for benzene, using tips of various radii. Knowing the values of γ from capillary rise measurements, and thence the respective values of a, f could be determined in each case. The resulting variation of f with $r/V^{1/3}$ has been fitted to a smoothing function to allow tabulation at close intervals [36].

†The actual statement by Tate is "Other things being equal, the weight of a drop of liquid is proportional to the diameter of the tube in which it is formed." See Refs. 34 and 35 for some discussion.

It is desirable to use $r/V^{1/3}$ values in the region of 0.6 to 1.2, where f is varying most slowly. The correct value for the surface tension is then given by

$$\gamma = \frac{mg}{2\pi r f} \tag{II-25}$$

It is to be noted that not only is the correction quite large, but for a given tip radius it depends on the nature of the liquid. It is thus *incorrect* to assume that the drop weights for two liquids are in the ratio of the respective surface tensions when the same size tip is used. Finally, correction factors for $r/V^{1/3} < 0.3$ have been determined, using mercury drops [37].

In employing this method, an important precaution to take is to use a tip that has been ground smooth at the end and is free from any nicks. In the case of liquids that do not wet the tip, r is the inside radius. Volatile liquids are studied in a closed system as described by Harkins and Brown [21] to minimize evaporation losses.

Since the drop volume method involves creation of surface, it is frequently used as a dynamic technique to study adsorption processes occurring over intervals of seconds to minutes. A commercial instrument delivers computer-controlled drops over intervals from 0.5 sec to several hours [38, 39]. Accurate determination of the surface tension is limited to drop times of a second or greater due to hydrodynamic instabilities on the liquid bridge between the detaching and residing drops [40].

An empirically determined relationship between drop weight and drop time does allow surface tensions to be determined for small surface ages [41].

B. The Ring Method

A method that has been rather widely used involves the determination of the force to detach a ring or loop of wire from the surface of a liquid. It is generally attributed to du Noüy [42]. As with all detachment methods, one supposes that a first approximation to the detachment force is given by the surface tension multiplied by the periphery of the surface detached. Thus, for a ring, as illustrated in Fig. II-11,

$$W_{\text{tot}} = W_{\text{ring}} + 4\pi R\gamma \tag{II-26}$$

Harkins and Jordan [43] found, however, that Eq. II-26 was generally in serious error and worked out an empirical correction factor in much the same way as was done for the drop weight method. Here, however, there is one additional variable so that the correction factor f now depends on two dimensionless ratios. Thus

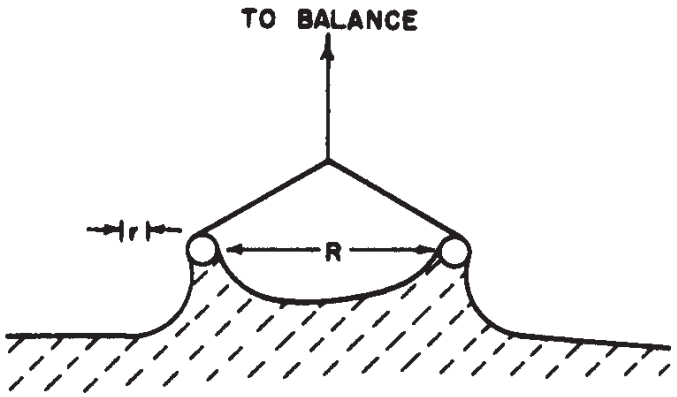

Fig. II-11. Ring method.

$$f = \frac{\gamma}{p} = f\left(\frac{R^3}{V}, \frac{R}{r}\right) \tag{II-27}$$

where p denotes the "ideal" surface tension computed from Eq. II-26, and V is the meniscus volume. The extensive tables of Harkins and Jordan, as recalculated by Huh and Mason [44] are summarized graphically in Fig. II-12, and it is seen that the simple equation may be in error by as much as 25%. Additional tables are given in Ref. 45.

Experimentally, the method is capable of good precision. Harkins and Jordan used

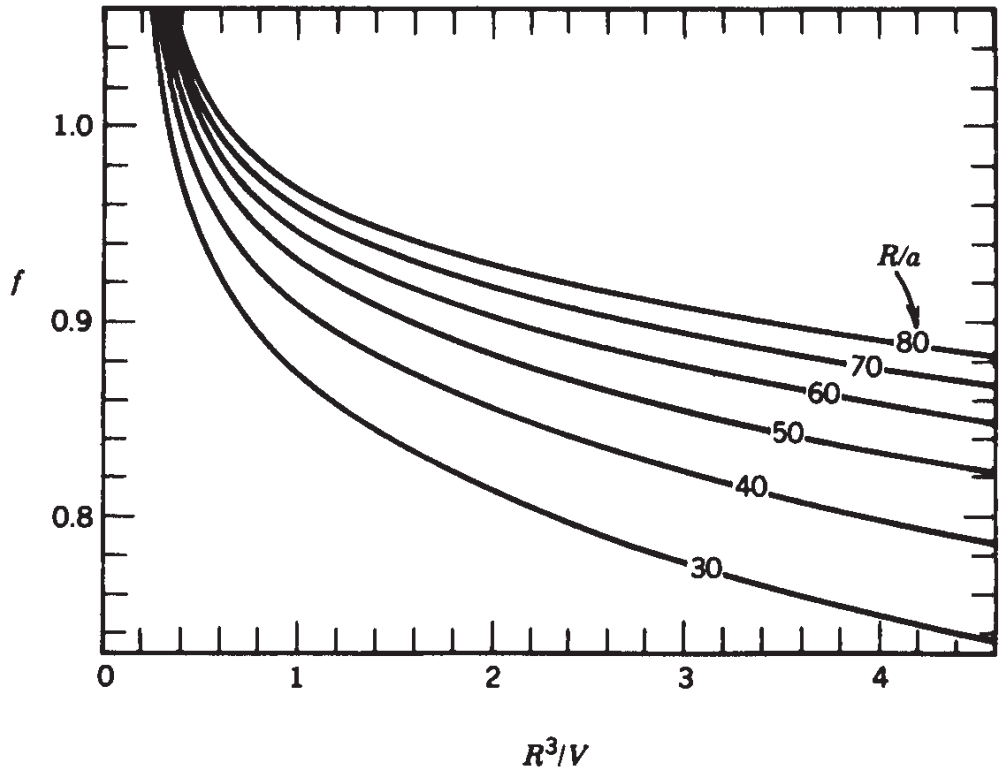

Fig. II-12. The factor f in the range of $R^3/V = 0.4$ to 4.5 and $R/a = 30$ to 80. (From Ref. 44.)

a chainomatic balance to determine the maximum pull, but a popular simplified version of the *tensiometer*, as it is sometimes called, makes use of a torsion wire and is quite compact. Among experimental details to mention are that the dry weight of the ring, which is usually constructed of platinum, is to be used, the ring should be kept horizontal (a departure of 1° was found to introduce an error of 0.5%, whereas one of 2.1° introduced an error of 1.6%), and care must be taken to avoid any disturbance of the surface as the critical point of detachment is approached. The ring is usually flamed before use to remove surface contaminants such as grease, and it is desirable to use a container for the liquid that can be overflowed so as to ensure the presence of a clean liquid surface. Additional details are given in Ref. 46.

A zero or near-zero contact angle is necessary; otherwise results will be low. This was found to be the case with surfactant solutions where adsorption on the ring changed its wetting characteristics, and where liquid-liquid interfacial tensions were measured. In such cases a Teflon or polyethylene ring may be used [47]. When used to study monolayers, it may be necessary to know the increase in area at detachment, and some calculations of this are available [48]. Finally, an alternative method obtains γ from the slope of the plot of W versus z, the elevation of the ring above the liquid surface [49].

C. Wilhelmy Slide Method

The methods so far discussed have required correction factors to the respective "ideal" equations. Yet there is one method, attributed to Wilhelmy [50] in 1863, that entails no such corrections and is very simple to use.

The basic observation is that a thin plate, such as a microscope cover glass or piece of platinum foil, will support a meniscus whose weight both as measured statically or by detachment is given very accurately by the "ideal" equation (assuming zero contact angle):

$$W_{\text{tot}} = W_{\text{plate}} + \gamma p \tag{II-28}$$

where p is the perimeter. The experimental arrangement is shown schematically in Fig. II-13. When used as a detachment method, the procedure is essentially the same as with the ring method, but Eq. II-28 holds to within 0.1% so that no corrections are needed [51, 52]. A minor, omitted term in Eq. II-28 allows for the weight of liquid directly under the plate (see Ref. 46).

It should be noted that here, as with capillary rise, there is an adsorbed film of vapor (see Section X-6D) with which the meniscus merges smoothly. The meniscus is not "hanging" from the plate but rather from a liquidlike film [53]. The correction for the weight of such film should be negligible, however.

An alternative and probably now more widely used procedure is to raise the liquid level gradually until it just touches the hanging plate suspended from a balance. The increase in weight is then noted. A general equation is

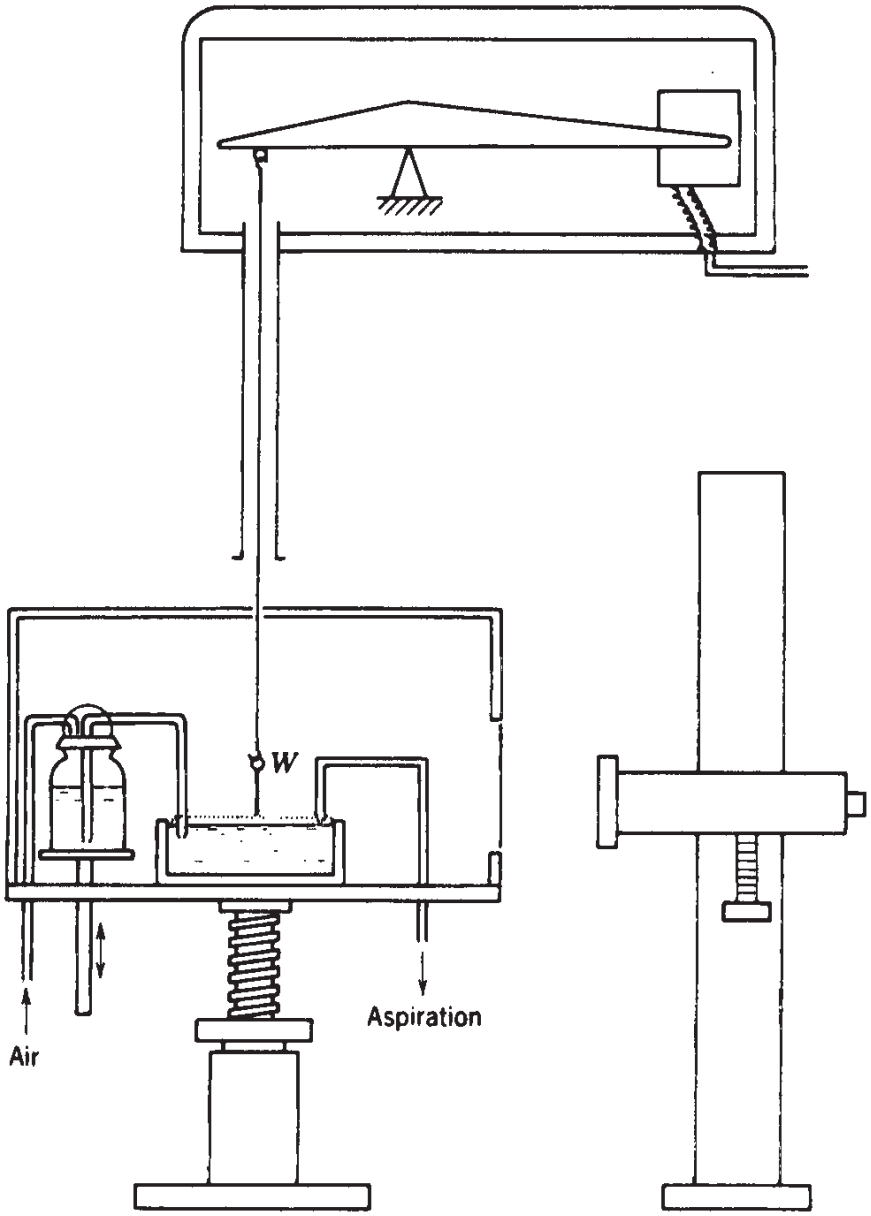

Fig. II-13. Apparatus for measuring the time dependence of interfacial tension (from Ref. 54). The air and aspirator connections allow for establishing the desired level of fresh surface. *W* denotes the Wilhelmy slide, suspended from a Cahn electrobalance with a recorder output.

$$\gamma \cos \theta = \frac{\Delta W}{p} \tag{II-29}$$

where ΔW is the change in weight of (i.e., force exerted by) the plate when it is brought into contact with the liquid, and p is the perimeter of the plate. The contact angle, if finite, may be measured in the same experiment [54]. Integration of Eq. II-12 gives

$$\left(\frac{h}{a}\right)^2 = 1 - \sin \theta \tag{II-30}$$

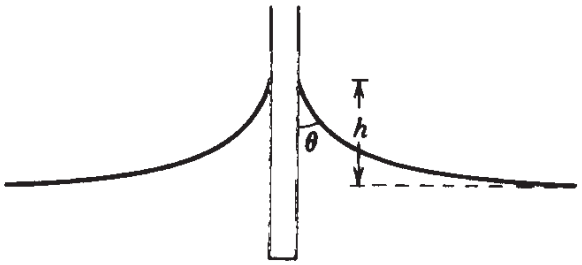

Fig. II-14. Meniscus profile for a nonwetting liquid.

where, as illustrated in Fig. II-14, h is the height of the top of the meniscus above the level liquid surface. Zero contact angle is preferred, however, if only the liquid surface tension is of interest; it may help to slightly roughen the plate, see Refs. 46 and 55.

As an example of the application of the method, Neumann and Tanner [54] followed the variation with time of the surface tension of aqueous sodium dodecyl sulfate solutions. Their results are shown in Fig. II-15, and it is seen that a slow but considerable change occurred.

A modification of the foregoing procedure is to suspend the plate so that it is partly immersed and to determine from the dry and immersed weights the meniscus weight. The procedure is especially useful in the study of surface adsorption or of monolayers, where a change in surface tension is to be measured. This application is discussed in some detail by Gaines [57]. Equation II-28 also applies to a wire or fiber [58].

The Wilhelmy slide has been operated in dynamic immersion studies to measure advancing and receding contact angles [59] (see Chapter X). It can also

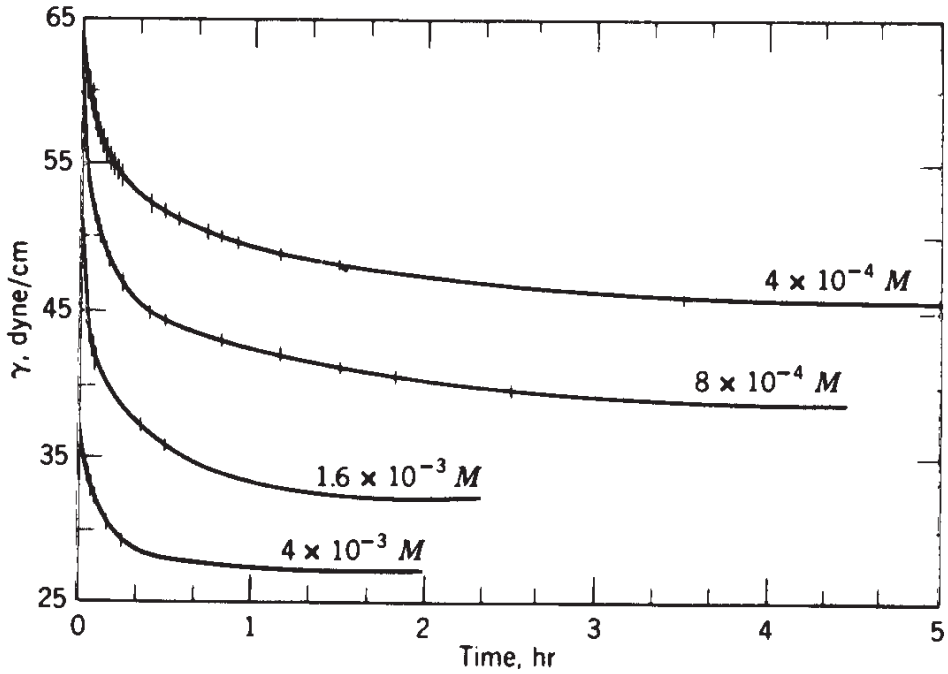

Fig. II-15. Variation with time of aqueous sodium dodecyl sulfate solutions of various concentrations (from Ref. 54). See Ref. 56 for later data with highly purified materials.

be used with a trapezoidal pulse applied to the barrier at a fluid–fluid interface to measure the transient response of the surface to a change in area [60].

7. Methods Based on the Shape of Static Drops or Bubbles

Small drops or bubbles will tend to be spherical because surface forces depend on the area, which decreases as the square of the linear dimension, whereas distortions due to gravitational effects depend on the volume, which decreases as the cube of the linear dimension. Likewise, too, a drop of liquid in a second liquid of equal density will be spherical. However, when gravitational and surface tensional effects are comparable, then one can determine in principle the surface tension from measurements of the shape of the drop or bubble. The variations situations to which Eq. II-16 applies are shown in Fig. II-16.

The general procedure is to form the drop or bubble under conditions such that it is not subject to disturbances and then to measure its dimensions or profile from a photograph or with digital image processing of video images (see Refs. 61, 62). The image analysis has recently been automated [62] to improve accuracy over manual analysis. In axisymmetric drop shape analysis of surface tension, the pendant drop geometry is preferable due to the ease with which large drops can be made axisymmetric. Sessile drops, however, are useful for studies of contact angles [63, 64] (see Chapter X). The greatest accuracy is achieved with fewer very accurate points on the drop surface rather than a large number of less reliable points [65].

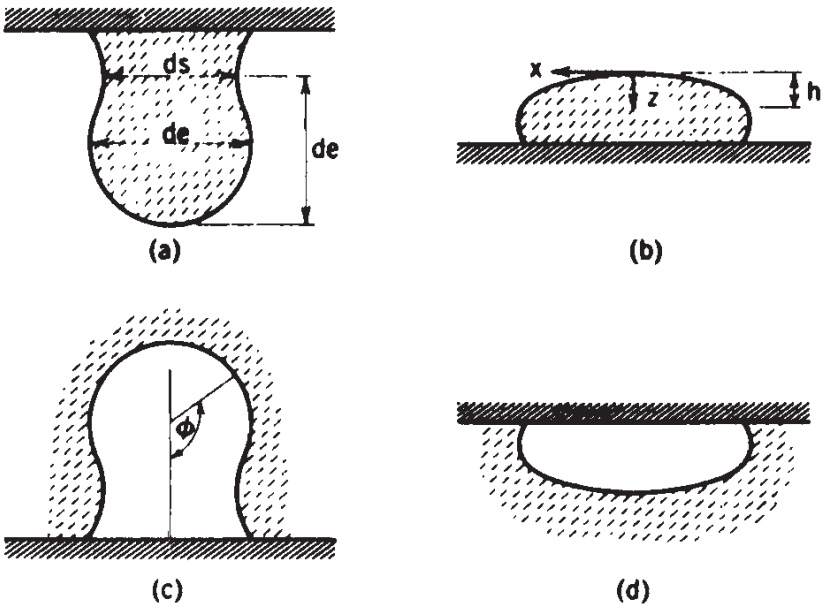

Fig. II-16. Shapes of sessile and hanging drops and bubbles: (*a*) hanging drop; (*b*) sessile drop; (*c*) hanging bubble; (*d*) sessile bubble.

A. Pendant Drop Method

A drop hanging from a tip (or a clinging bubble) elongates as it grows larger because the variation in hydrostatic pressure ΔP eventually becomes appreciable in comparison with that given by the curvature at the apex. As in the case of a meniscus, it is convenient to write Eq. II-12 in the form of Eq. II-17, where in the present case, the dimensionless parameter β is negative. A profile calculated from Eq. II-17 for the case of $\beta = -0.45$ is given in Table II-3 [66]. The best value of β for a given drop can be determined by profile matching (see further below), but some absolute quantity such as b must also be measured in order to obtain an actual γ value.

An alternative to obtaining β directly involves defining some more convenient shape-dependent function, and an early but still very practical method is the following. We define a shape-dependent quantity as $S = d_s/d_e$; as indicated in Fig. II-16, d_e is the equatorial diameter and d_s is the diameter measured at a distance d_e up from the bottom of the drop. The hard-to-measure size parameter b in Eq. II-17 is combined with β by defining the quantity $H = -\beta(d_e/b)^2$. Thus

$$\gamma = \frac{-\Delta\rho\, g b^2}{\beta} = \frac{-\Delta\rho\, g d_e^2}{\beta(d_e/b)^2} = \frac{\Delta\rho\, g d_e^2}{H} \tag{II-31}$$

The relationship between the shape-dependent quantity H and the experimentally measurable quantity S originally was determined empirically [66], but a set of quite accurate $1/H$ versus S values were later obtained by Niederhauser and Bartell [67] (see also Refs. 34 and 68) and by Stauffer [69].

A set of pendant drop profiles is shown in Fig. II-17 as an illustration of the range of shapes that may be observed. It has been pointed out that for practical reasons, the size of the tip from which the drop is suspended should be such that r/a is about 0.5 or less [66].

A modern alternative procedure involves computer matching of the entire drop profile to a best fitting theoretical curve; in this way the entire profile is used, rather than just d_s and d_e, so that precision is increased. Also, drops whose d_s is not measurable (how does this happen?) can be used. References 61 and 71–74 provide examples of this type of approach.

The automated pendant drop technique has been used as a film balance to study the surface tension of insoluble monolayers [75] (see Chapter IV). A motor-driven syringe allows changes in drop volume to study surface tension as a function of surface areas as in conventional film balance measurements. This approach is useful for materials available in limited quantities and it can be extended to study monolayers at liquid–liquid interfaces [76].

B. Sessile Drop or Bubble Method

The cases of the sessile drop and bubble are symmetrical, as illustrated in Fig. II-16. The profile is also that of a meniscus; β is now positive and, as an

TABLE II-3
Solutions to Eq. II-17 for $\beta = -0.45$

ϕ^a	x/b	z/b
0.099944	0.099834	0.004994
0.199551	0.198673	0.019911
0.298488	0.295547	0.044553
0.396430	0.389530	0.078600
0.493058	0.479762	0.121617
0.588070	0.565464	0.173072
0.681175	0.645954	0.232352
0.772100	0.720657	0.298779
0.860590	0.789108	0.371635
0.946403	0.850958	0.460175
1.029319	0.905969	0.533649
1.109130	0.954013	0.621322
1.185644	0.995064	0.712480
1.258681	1.029190	0.806454
1.328069	1.056542	0.902619
1.393643	1.077347	1.000413
1.455242	1.091895	1.099333
1.512702	1.100530	1.198946
1.565856	1.103644	1.298886
1.614526	1.101667	1.398856
1.658523	1.095060	1.498630
1.697641	1.084311	1.598044
1.731653	1.069933	1.697000
1.760310	1.052460	1.795458
1.783338	1.032445	1.893432
1.800443	1.010466	1.990986
1.811310	0.987123	2.088223
1.815618	0.963039	2.185279
1.813050	0.938868	2.282314
1.803321	0.915293	2.379495
1.786207	0.893023	2.476982
1.761593	0.872791	2.574912
1.729517	0.855344	2.673373
1.690226	0.841424	2.772393

[a]The angle ϕ is in units of $360/2\pi$ or 57.295°.

example, the solution to Eq. II-17 for $\beta = 0.5$ is given in Ref. 77 (note also Table II-1).

The usual experimental situation is that of a sessile drop and, as with the pendant drop, it is necessary to determine a shape parameter and some absolute length. Thus β may be determined by profile fitting, and z_e measured, where z_e is the distance from the plane at $\phi = 90$ to the apex. If the drop rests with

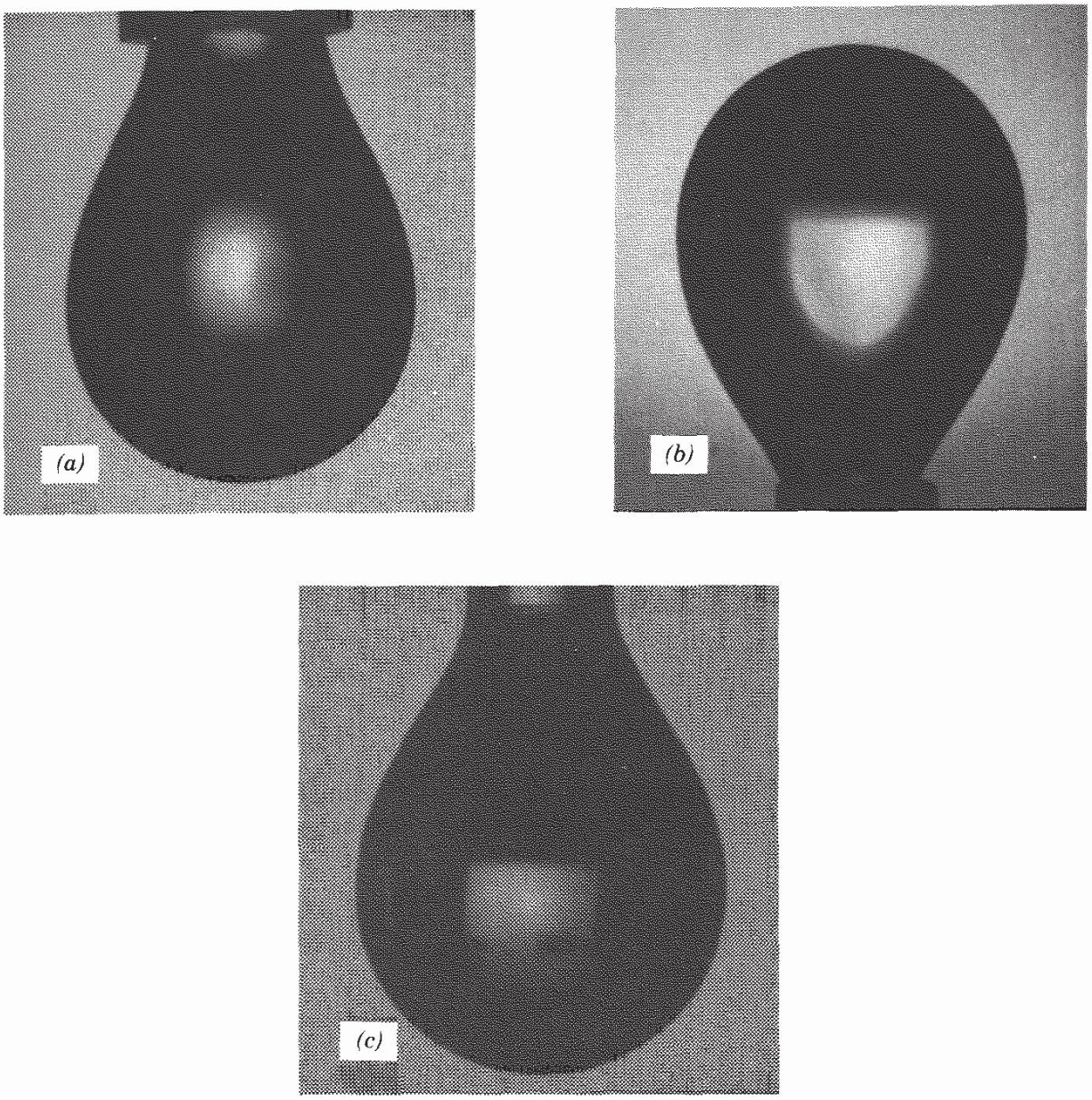

Fig. II-17. Pendant drops: (*a*) water; (*b*) benzene/water; (*c*) formamide. The measurements were at 21°. [Courtesy A. W. Neumann (see also Ref. 70).]

a contact angle of less than 90°, there is no z_e and, instead, the control angle and the total height of the drop can be measured. Some of the specific procedures that have been used are found in Refs. 71–74 and 77–79. The sessile drop method has been used to follow surface tension as a function of time, as with sodium laurate solutions [80], the surface tension of molten metals [81–83] and liquid-liquid interfacial tensions [70, 73].

The case of very large drops or bubbles is easy because only one radius of curvature (that in the plane of the drawings) is considered. Equation II-12 then becomes

$$\Delta\rho g y = \gamma \frac{y''}{(1 + y'^2)^{3/2}}$$

or

$$\frac{2y}{a^2} = \frac{p\,dp/dy}{(1+p^2)^{3/2}} \tag{II-32}$$

where $p = dy/dx$. Integration gives

$$\frac{y^2}{a^2} = \frac{-1}{(1+p^2)^{1/2}} + \text{const} \tag{II-33}$$

Since h denotes the distance from the apex to the equatorial plane, then at $y = h$, $p = \infty$, and Eq. II-33 becomes

$$\frac{y^2}{a^2} - \frac{h^2}{a^2} = \frac{-1}{(1+p^2)^{1/2}}$$

Furthermore, at $y = 0$, $p = 0$, from which it follows that $h^2/a^2 = 1$, or $h = a$,

$$\gamma = \frac{\Delta\rho\, g h^2}{2} \tag{II-34}$$

This very simple result is independent of the value of the contact angle because the configuration involved is only that between the equatorial plane and the apex.

Very small sessile drops have a shape that depends on the line tension along the circular contact line; if large enough it induces a dewetting transition detaching the drop from the surface [84].

C. Sources of Other Deformed Shapes

The discussion so far has been of interfaces in a uniform gravitational field. There are several variants from this situation, some of which are useful in the measurement of liquid-liquid interfacial tensions where these are very small. Consider the case of a drop of liquid A suspended in liquid B. If the density of A is less than that of B, on rotating the whole mass, as illustrated in Fig. II-18, liquid A will go to the center, forming a drop astride the axis of revolution. With increasing speed of revolution, the drop of A elongates, since centrifugal force increasingly opposes the surface tensional drive toward minimum interfacial area. In brief, the drop of A deforms from a sphere to a prolate ellipsoid. At a sufficiently high speed of revolution, the drop approximates to an elongated cylinder.

The general analysis, while not difficult, is complicated; however, the limiting case of the very elongated, essentially cylindrical drop is not hard to treat. Consider a section of the elongated cylinder of volume V (Fig. II-18*b*). The centrifugal force on a volume element is $\omega^2 r\,\Delta\rho$, where ω is the speed of revolution and $\Delta\rho$ the difference in density. The potential energy at distance r from the axis of revolution is then $\omega^2 r^2 \Delta\rho/2$, and the total potential energy for the

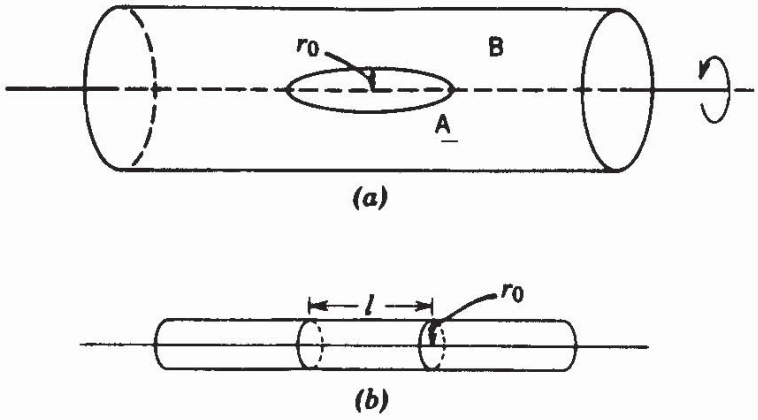

Fig. II-18. Illustration of the rotating drop method.

cylinder of length l is $l\int_0^{r_0}(\omega^2 r^2\,\Delta\rho/2)2\pi r\,dr = \pi\omega^2\,\Delta\rho\,r_0^4 l/4$. The interfacial free energy is $2\pi r_0 l\gamma$. The total energy is thus

$$E = \frac{\pi\omega^2\,\Delta\rho\,r_0^4 l}{4} + 2\pi r_0 l\gamma = \frac{\omega^2\,\Delta\rho\,r_0^2 V}{4} + \frac{2V\gamma}{r_0}$$

since $V = \pi r_0^2 l$. Setting $dE/dr_0 = 0$, we obtain

$$\gamma = \frac{\omega^2\,\Delta\rho\,r_0^3}{4} \tag{II-35}$$

Equation II-35 has been called Vonnegut's equation [85].

Princen and co-workers have treated the more general case where ω is too small or γ too large to give a cylindrical profile [86] (see also Refs. 87 and 88). In such cases, however, a correction may be needed for buoyancy and Coriolis effects [89]; it is best to work under conditions such that Eq. II-35 applies. The method has been used successfully for the measurement of interfacial tensions of 0.001 dyn/cm or lower [90, 91].

Small interfacial tensions may also be measured from the deformation of a drop suspended in a liquid having a similar density [92]. The distortion of drops and bubbles placed in shearing flows of liquids was first investigated theoretically by G. I. Taylor in 1934, who also conducted a series of careful experiments. He established that the parameter measuring the distorting forces due to the flow relative to the interfacial tension opposing the distortion is a capillary number, $Ca = U\mu/\gamma$, where U is the fluid velocity, μ the viscosity, and γ the interfacial tension. For unbounded simple shear flow, U is replaced by Ga, where G is the shear rate and a the radius of the undistorted drop. Taylor carried out a perturbation expansion for small Ca, showing the first effects of shape distortion. Many theoretical and experimental studies have extended his work to finite internal viscosity, more general flows, and large deformation or breakup. This work is reviewed by Rallison [93] and Stone [93a]. An initially

spherical drop will deform to a spheroid of major axis ℓ and minor axis b; the degree of deformation is defined by $D = (\ell - b)/(\ell + b)$. The deformation of a drop of radius r in an electric field E is

$$D = \frac{9\epsilon_0 \epsilon r E^2}{16\gamma} \tag{II-36}$$

where ϵ_0 is the permittivity of vacuum (8.854×10^{-12} $C^2N^{-1}m^{-2}$, and ϵ is the dielectric constant of the outer fluid (that for the drop is assumed to be high) [94–96]. This effect was noted by Lord Kelvin [97]. Finally, the profiles of nonaxisymmetric drops including inclined pendant [98] and sessile [99] drops have been calculated.

In the converse situation free of gravity, a drop assumes a perfectly spherical shape. At one point, the U.S. Space program tested this idea with the solidification of ball bearings from molten metal drops in microgravity conditions.

An interesting application of capillarity and drops in fields occurs in inkjet printing technology. In this process, illustrated in Fig. II-19, ink resides in a small square chamber with a meniscus balanced at the exit orifice by the pressure in the reservoir and capillary forces. In the wall opposite the orifice is a thin film resistor that, upon heating at 10^8°C/sec, causes rapid growth of a vapor bubble that ejects a drop of ink through the orifice (Fig. II-19*b*). The chamber refills and the process is repeated. The newest printers achieve a repetition frequency of 8000 Hz by carefully controlling the refilling process [100].

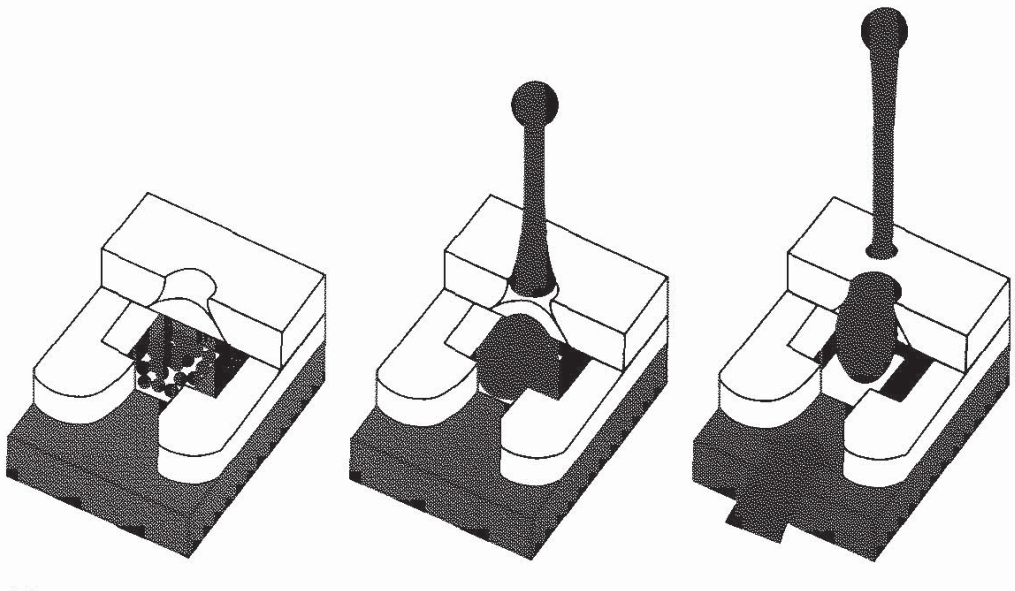

(*a*) (*b*) (*c*)

Fig. II-19. The drop ejection process in an inkjet printer: (*a*) bubble nucleation; (*b*) bubble growth and drop ejection; (*c*) refill. [From J. H. Bohórquez, B. P. Canfield, K. J. Courian, F. Drogo, C. A. E. Hall, C. L. Holstun, A. R. Scandalis, and M. E. Shepard, *Hewlett-Packard J.* **45**(1), 9–17 (Feb. 1994). Copyright 1994, Hewlett-Packard Company. Reproduced with permission.]

8. Dynamic Methods of Measuring Surface Tension

The profound effect of surface active agents on the surface tension of a liquid motivate the study of their adsorption at liquid surfaces through the dynamic measurement of surface tension Recent computer-controlled devices have enabled such studies via the pulsating bubble method described in Section II-5 and the drop weight technique (Section II-6A). These techniques are generally limited to the study of surface tensions varying over time periods of seconds to minutes. It is of interest to study surface aging and relaxation effects on a very short time scale, and for this more rapid dynamic methods are needed. Two good reviews of dynamic surface tension techniques by Miller and co-workers and by Chang and Franses appear in Refs. 101 and 102. We briefly describe three of these techniques below.

A. Flow Methods

A jet emerging from a noncircular orifice is mechanically unstable, not only with respect to the eventual breakup into droplets discussed in Section II-3, but, more immediately, also with respect to the initial cross section not being circular. Oscillations develop in the jet since the momentum of the liquid carries it past the desired circular cross section. This is illustrated in Fig. II-20.

The mathematical treatment was first developed by Lord Rayleigh in 1879, and a more exact one by Bohr has been reviewed by Sutherland [103], who gives the formula

$$\gamma_{app} = \frac{4\rho v^2(1 + 37b^2/24r^2)}{6r\lambda^2(1 + 5\pi^2 r^2/3\lambda^2)} \tag{II-37}$$

where ρ is the density of the liquid, v is the volume velocity, λ is the wavelength, r is the sum of the minimum and maximum half-diameters, and b is their difference. The required jet dimensions were determined optically, and a typical experiment would make use of jets of about 0.03 cm in size and velocities of about 1 cm^3/sec, giving λ values of around 0.5 cm. To a first approximation, the surface age at a given node is

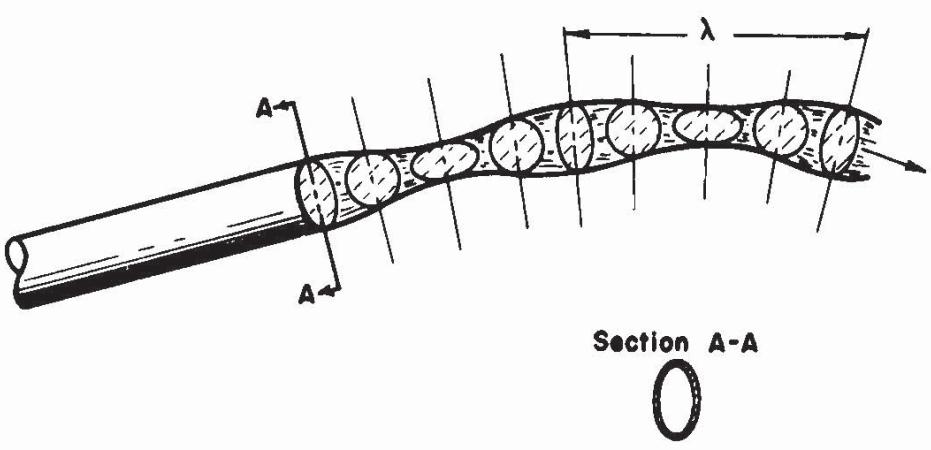

Fig. II-20. Oscillations in an elliptical jet.

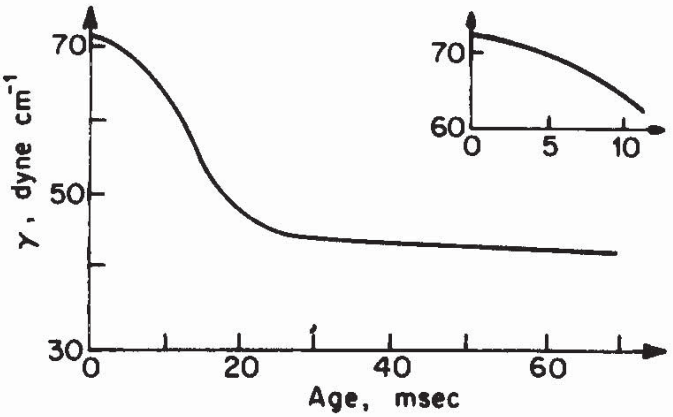

Fig. II-21. Surface tension as a function of age for 0.05 g/100 cm^3 of sodium di(2-ethylhexyl)sulfosuccinate solution determined with various types of jet orifices [109].

just the distance from the orifice divided by the linear jet velocity and, in the preceding example, would be about 1 msec per wavelength.

It was determined, for example, that the surface tension of water relaxes to its equilibrium value with a relaxation time of 0.6 msec [104]. The oscillating jet method has been useful in studying the surface tension of surfactant solutions. Figure II-21 illustrates the usual observation that at small times the jet appears to have the surface tension of pure water. The slowness in attaining the equilibrium value may partly be due to the times required for surfactant to diffuse to the surface and partly due to chemical rate processes at the interface. See Ref. 105 for similar studies with heptanoic acid and Ref. 106 for some anomalous effects.

For times below about 5 msec a correction must be made to allow for the fact that the surface velocity of the liquid *in* the nozzle is zero and takes several wavelengths to increase to the jet velocity after emerging from the nozzle. Correction factors have been tabulated [107, 108]; see also Ref. 109.

The oscillating jet method is not suitable for the study of liquid-air interfaces whose ages are in the range of tenths of a second, and an alternative method is based on the dependence of the shape of a falling column of liquid on its surface tension. Since the hydrostatic head, and hence the linear velocity, increases with h, the distance away from the nozzle, the cross-sectional area of the column must correspondingly decrease as a material balance requirement. The effect of surface tension is to oppose this shrinkage in cross section. The method is discussed in Refs. 110 and 111. A related method makes use of a falling sheet of liquid [112].

Another oscillatory method makes use of a drop acoustically levitated in a liquid. The drop is made to oscillate in shape, and the interfacial tension can be calculated from the resonance frequency [113].

B. Capillary Waves

The wavelength of ripples on the surface of a deep body of liquid depends on the surface tension. According to a formula given by Lord Kelvin [97],

$$v^2 = \frac{g\lambda}{2\pi} + \frac{2\pi\gamma}{\rho\lambda}$$

$$\gamma = \frac{\lambda^3\rho}{2\pi\tau^2} - \frac{g\lambda^2\rho}{4\pi^2} \qquad \text{(II-38)}$$

where v is the velocity of propagation, λ is the wavelength, and τ is the period of the ripples. For water there is a minimum velocity of about 0.5 mph (mi/hr) for $\lambda = 1.7$ cm; for $\lambda = 0.1$ cm, it is 1.5 mph, whereas for $\lambda = 10^5$ cm, it is 89 mph!

Experimentally, the waves are measured as standing waves, and the situation might be thought to be a static one. However, individual elements of liquid in the surface region undergo a roughly circular motion, and the surface is alternately expanded and compressed. As a consequence, damping occurs even with a pure liquid, and much more so with solutions or film-covered surfaces for which transient surface expansions and contractions may be accompanied by considerable local surface tension changes and by material transport between surface layers. Hansen has reviewed the subject [114]. A more detailed discussion is deferred to Chapter IV, but it should be mentioned here that capillary waves are spontaneously present because of small temperature and hence density fluctuations. These minute waves (about 5 Å amplitude and 0.1 mm wavelength) can be detected by laser light-scattering techniques. The details are beyond the scope of this text; they are discussed in Refs. 115–118. Both liquid-air and liquid-liquid surface tensions can be measured, as well as the rate of damping of waves.

C. Maximum Bubble Pressure Method

A recent design of the maximum bubble pressure instrument for measurement of dynamic surface tension allows resolution in the millisecond time frame [119, 120]. This was accomplished by increasing the system volume relative to that of the bubble and by using electric and acoustic sensors to track the bubble formation frequency. Miller and co-workers also assessed the hydrodynamic effects arising at short bubble formation times with experiments on very viscous liquids [121]. They proposed a correction procedure to improve reliability at short times. This technique is applicable to the study of surfactant and polymer adsorption from solution [101, 120].

9. Surface Tension Values as Obtained by Different Methods

The surface tension of a pure liquid should and does come out to be the same irrespective of the method used, although difficulties in the mathematical treatment of complex phenomena can lead to apparent discrepancies. In the case of solutions, however, dynamic methods, including detachment ones, often tend

TABLE II-4
Surface Tension Values[a]

Liquid	Temperature	γ (dyn/cm mN/m)
Liquid–Vapor Interfaces		
Water[b]	20°C	72.94
	21.5°C	72.75
	25°C	72.13
Organic compounds		
Methylene iodide[c]	20°C	67.00
	21.5°C	63.11
Glycerine[d]	24°C	62.6
	20°C	48.09
Ethylene glycol[e]	25°C	47.3
	40°C	46.3
Dimethyl sulfoxide[f]	20°C	43.54
Propylene carbonate[g]	20°C	41.1
1-Methyl naphthalene[h]	20°C	38.7
Dimethyl aniline[i]	20°C	36.56
Benzene[b]	20°C	28.88
	30°C	27.56
Toluene[b]	20°C	28.52
Chloroform[b]	25°C	26.67
Propionic acid[b]	20°C	26.69
Butyric acid[b]	20°C	26.51
Carbon tetrachloride[b]	25°C	26.43
Butyl acetate[j]	20°C	25.09
Diethylene glycol[k]	20°C	30.9
Nonane[b]	20°C	22.85
Methanol[b]	20°C	22.50
Ethanol[b]	20°C	22.39
	30°C	21.55
Octane[b]	20°C	21.62
Heptane[b]	20°C	20.14
Ether[b]	25°C	20.14
Perfluoromethylcyclohexane[b]	20°C	15.70
Perfluoroheptane[b]	20°C	13.19
Hydrogen sulfide[l]	20°C	12.3
Perfluoropentane[b]	20°C	9.89
Dodecane[gg]	22°C	25.44
Polydimethyl siloxane, MW 3900[ff]	20°C	20.47
	20°C	21.01

TABLE II-4 (*Continued*)

Liquid	Temperature	γ (dyn/cm mN/m)
Liquid–Vapor Interfaces		
Low-boiling substances		
$^4He^m$	1K	0.365
$H_2{}^n$	20 K	2.01
$D_2{}^n$	20 K	3.54
$N_2{}^o$	75 K	9.41
Ar^o	90 K	11.86
$CH_4{}^b$	110 K	13.71
$F_2{}^b$	85 K	14.84
$O_2{}^b$	77 K	16.48
Metals		
Hg^b	20°C	486.5
	25°C	485.5
	30°C	484.5
Na^s	130°C	198
Ba^t	720°C	226
Sn^u	332°C	543.8
Salts		
$NaCl^y$	1073°C	115
$KClO_3{}^z$	368°C	81
$KNCS^z$	175°C	101.5
$C_2H_6{}^p$	180.6 K	16.63
Xe^q	163 K	18.6
N_2O^p	182.5 K	24.26
$Cl_2{}^b$	−30°C	25.56
$NOCl^b$	−10°C	13.71
$Br_2{}^r$	20°C	31.9
Ag^v	1100°C	878.5
Cu^w	mp	1300
Ti^x	1680°C	1588
Pt^w	mp	1800
Fe^w	mp	1880
$NaNO_3{}^{aa}$	308°C	116.6
$K_2Cr_2O_7{}^z$	397°C	129
$Ba(NO_3)_2{}^{aa}$	595°C	134.8

to give high values. Padday and Russell discuss this point in some detail [122]. The same may be true of interfacial tensions between partially miscible liquids.

The data given in Table II-4 were selected with the purpose of providing a working stock of data for use in problems as well as a convenient reference to

TABLE II-4 (*Continued*)

Liquid	Temperature	γ (dyn/cm mN/m)
Liquid–Liquid Interface		
Liquid 1: water		
n-Butyl alcohol[bb]	20°C	1.8
Ethyl acetate[bb]	20°C	6.8
Heptanoic acid[cc]	20°C	7.0
Benzaldehyde[aa]	20°C	15.5
Liquid 1: mercury		
Water[dd]	20°C	415
	25°C	416
Ethanol[cc]	20°C	389
n-Hexane[cc]	20°C	378
Liquid 1: fluorocarbon polymer		
Benzene[ee]	25°C	7.8
Liquid 1: diethylene glycol		
n-Heptane[j]	20°C	10.6
Nitrobenzene[bb]	20°C	25.2
Benzene[cc]	20°C	35.0
Carbon tetrachloride[cc]	20°C	45.0
n-Heptane[cc]	20°C	50.2
n-Heptane[cc]	20°C	378
Benzene[dd]	20°C	357
Water[ee]	25°C	57
n-Decane[k]	20°C	11.6

[a]Extensive compilations are given by J. J. Jasper, *J. Phys. Chem. Ref. Data*, **1,** 841 (1972) and G. Korosi and E. sz. Kováts, *J. Chem. Eng. Data*, **26,** 323 (1981).

[b]A. G. Gaonkar and R. D. Neuman, *Colloids & Surfaces*, **27,** 1 (1987) (contains an extensive review of the literature); V. Kayser, *J. Colloid Interface Sci.*, **56,** 622 (1972).

[c]R. Grzeskowiak, G. H. Jeffery, and A. I. Vogel, *J. Chem. Soc.*, **1960,** 4728.

[d]Ref. 61.

[e]Ref. 41.

[f]H. L. Clever and C. C. Snead, *J. Phys. Chem.*, **67,** 918 (1963).

[g]M. K. Bernett, N. L. Jarvis, and W. A. Zisman, *J. Phys. Chem.*, **66,** 328 (1962).

[h]A. N. Gent and J. Schultz, *J. Adhes.*, **3,** 281 (1972).

[i]Ref. 20.

[j]J. B. Griffin and H. L. Clever, *J. Chem. Eng. Data*, **5,** 390 (1960).

[k]G. L. Gaines, Jr., and G. L. Gaines III, *J. Colloid Interface Sci.*, **63,** 394 (1978).

TABLE II-4 (*Continued*)

[l]C. S. Herrick and G. L. Gaines, Jr., *J. Phys. Chem.*, **77,** 2703 (1973).
[m]K. R. Atkins and Y. Narahara, *Phys. Rev.*, **138,** A437 (1965).
[n]V. N. Grigor'ev and N. S. Rudenko, *Zh. Eksperim. Teor. Fiz.*, **47,** 92 (1964) (through *Chem. Abstr.*, **61,** 12669[g] (1964)).
[o]D. Stansfield, *Proc. Phys. Soc.*, **72,** 854 (1958).
[p]A. J. Leadbetter, D. J. Taylor, and B. Vincent, *Can. J. Chem.*, **42,** 2930 (1964).
[q]A. J. Leadbetter and H. E. Thomas, *Trans. Faraday Soc.*, **61,** 10 (1965).
[r]M. S. Chao and V. A. Stenger, *Talanta*, **11,** 271 (1964) (through *Chem. Abstr.*, **60,** 4829[g] (1964)).
[s]C. C. Addison, W. E. Addison, D. H. Kerridge, and J. Lewis, *J. Chem. Soc.*, **1955,** 2262.
[t]C. C. Addison, J. M. Coldrey, and W. D. Halstead, *J. Chem. Soc.*, **1962,** 3868.
[u]J. A. Cahill and A. D. Kirshenbaum, *J. Inorg. Nucl. Chem.*, **26,** 206 (1964).
[v]I. Lauerman, G. Metzger, and F. Sauerwald, *Z. Phys. Chem.*, **216,** 42 (1961).
[w]B. C. Allen, *Trans. Met. Soc. AIME*, **227**, 1175 (1963).
[x]J. Tille and J. C. Kelley, *Brit. J. Appl. Phys.*, **14**(10), 717 (1963).
[y]J. D. Patdey, H. R. Chaturvedi, and R. P. Pandey, *J. Phys. Chem.*, **85,** 1750 (1981).
[z]J. P. Frame, E. Rhodes, and A. R. Ubbelohde, *Trans. Faraday Soc.*, **55,** 2039 (1959).
[aa]C. C. Addison and J. M. Coldrey, *J. Chem. Soc.*, **1961,** 468.
[bb]D. J. Donahue and F. E. Bartell, *J. Phys. Chem.*, **56,** 480 (1952).
[cc]L. A. Girifalco and R. J. Good, *J. Phys. Chem.*, **61,** 904 (1957).
[dd]E. B. Butler, *J. Phys. Chem.*, **67,** 1419 (1963).
[ee]F. M. Fowkes and W. M. Sawyer, *J. Chem. Phys.*, **20,** 1650 (1952).
[ff]Q. S. Bhatia, J. K. Chen, J. T. Koberstein, J. E. Sohn, and J. A. Emerson, *J. Colloid Interface Sci.*, **106,** 353 (1985).
[gg]P. Cheng, D. Li, L. Boruvka, Y. Rotenburg, and A. W. Neumann, *Colloids & Surf.*, **43**, 151 (1990).

surface tension values for commonly studied interfaces. In addition, a number of values are included for uncommon substances or states of matter (e.g., molten metals) to provide a general picture of how this property ranges and of the extent of the literature on it. While the values have been chosen with some judgment, they are not presented as critically selected best values. Finally, many of the references cited in the table contain a good deal of additional data on surface tensions at other temperatures and for other liquids of the same type as the one selected for entry in the table. A useful empirical relationship for a homologous series of alkane derivatives is [123]

$$\gamma = \gamma_\infty - \frac{k}{M^{2/3}} \tag{II-39}$$

Series of the type $C_nH_{2n+1}X$ were studied. For X = CH_2Cl, k and γ_∞ were 304 and 37.44 dyn/cm, respectively, and for X = $COOCH_3$, k and γ_∞ were 254 and 35.47 dyn/cm, again respectively.

10. Problems

1. Derive Eq. II-3 using the "surface tension" point of view. *Suggestion:* Consider the sphere to be in two halves, with the surface tension along the join balancing the force due to ΔP, which would tend to separate the two halves.

2. The diagrams in Fig. II-22 represent capillaries of varying construction and arrangement. The diameter of the capillary portion is the same in each case, and all of the capillaries are constructed of glass, unless otherwise indicated. The equilibrium rise for water is shown at the left. Draw meniscuses in each figure to correspond to (*a*) the level reached by water rising up the clean, dry tube and (*b*) the level to which the water would recede after having been sucked up to the end of the capillary. The meniscuses in the capillary may be assumed to be spherical in shape.

3. Show that the second term in Eq. II-15 does indeed correct for the weight of the meniscus. (Assume the meniscus to be hemispherical.)

4. Calculate to 1% accuracy the capillary rise for water at 20°C in a 1.2-cm-diameter capillary.

5. Referring to the numerical example following Eq. II-18, what would be the surface tension of a liquid of density 1.423 g/cm^3 (2-bromotoluene), the rest of the data being the same?

6. Derive Eq. II-5.

7. Derive Eq. II-14 from an exact analysis of the meniscus profile. *Hint:* Start with Eq. II-12 and let $p = y'$, where $y'' = p\,dp/dy$. The total weight W is then given by $W = 2\Delta\rho g\pi \int_0^r xy\,dx$.

8. Derive Eq. II-13. *Hint:* Use Eqs. II-4, II-5, and II-7 and note an alternative statement for R_2.

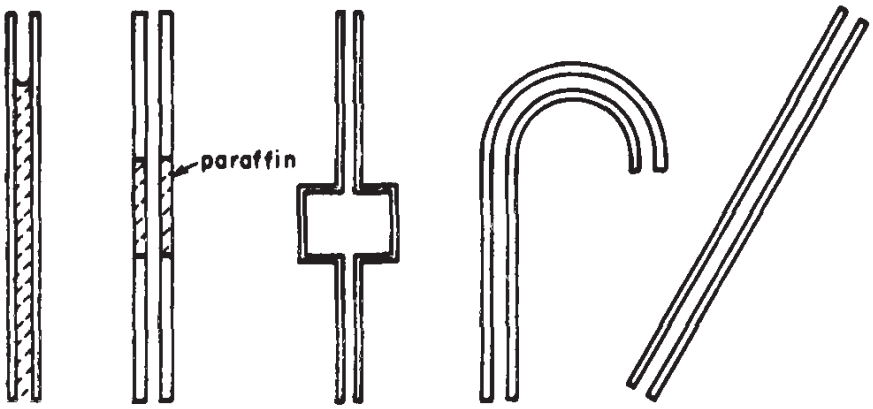

Fig. II-22

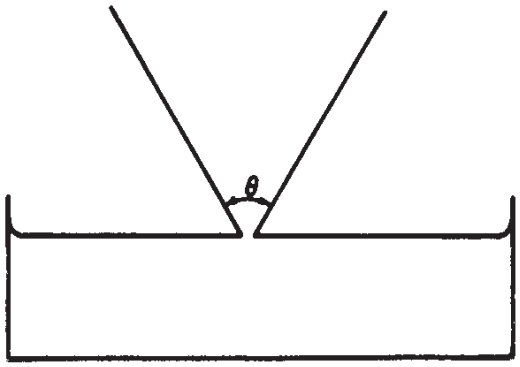

Fig. II-23.

9. Obtain Eq. II-14 from Eq. II-11. It is interesting that the former equation is exact although it has been obtained in this case from Eq. II-11, which is approximate.

10. The surface tension of a liquid that wets glass is measured by determining the height Δh between the levels of the two meniscuses in a U-tube having a small radius r_1 on one side and a larger radius r_2 on the other. The following data are known: $\Delta h = 1.90 \times 10^{-2}$ m, $r_1 = 1.00 \times 10^{-3}$ m, $r_2 = 1.00 \times 10^{-2}$ m, $\rho = 950$ kg/m^3 at 20°C. Calculate the surface tension of the liquid using (*a*) the simple capillary rise treatment and (*b*) making the appropriate corrections using Eqs. II-19 and II-20.

11. The surface tension of a liquid is determined by the drop weight method. Using a tip whose outside diameter is 5×10^{-3} m and whose inside diameter is 2.5×10^{-3} m, it is found that the weight of 20 drops is 7×10^{-4} kg. The density of the liquid is 982.4 kg/m^3, and it wets the tip. Using $r/V^{1/3}$, determine the appropriate correction factor and calculate the surface tension of this liquid.

12. Derive the equation for the capillary rise between parallel plates, including the correction term for meniscus weight. Assume zero contact angle, a cylindrical meniscus, and neglect end effects.

13. Derive, from simple considerations, the capillary rise between two parallel plates of infinite length inclined at an angle of θ to each other, and meeting at the liquid surface, as illustrated in Fig. II-23. Assume zero contact angle and a circular cross section for the meniscus. Remember that the area of the liquid surface changes with its position.

14. The following values for the surface tension of a $10^{-4}M$ solution of sodium oleate at 25°C are reported by various authors: (*a*) by the capillary rise method, $\gamma = 43$ mN/m; (*b*) by the drop weight method, $\gamma = 50$ mN/m; and (*c*) by the sessile drop method, $\gamma = 40$ mN/m. Explain how these discrepancies might arise. Which value should be the most reliable and why?

15. Derive Eq. II-30.

16. Molten naphthalene at its melting point of 82°C has the same density as does water at this temperature. Suggest two methods that might be used to determine the naphthalene-water interfacial tension. Discuss your suggestions sufficiently to show that the methods will be reasonably easy to carry out and should give results good to 1% or better.

17. Using Table II-3, calculate S and $1/H$ for $\beta = -0.45$ for a pendant drop. *Hint:* x/b in the table is at a maximum when x is the equatorial radius.

18. This problem may be worked as part (*a*) only or as part (*b*) only; it is instructive, however, to work all three parts.

(*a*) A drop of liquid *A*, of density 1.01 g/cm^3, rests on a flat surface that it does not wet but contacts with an angle θ (measured in the liquid phase). The height of the drop above the surface is 0.22 cm, and its largest diameter is 0.67 cm. Its shape corresponds to $\beta = 80$ (see Table II-1). Calculate the surface tension of liquid *A* and its value of θ.

(*b*) Plot the profile for the drop of liquid *A* as z (in cm) versus x (in cm).

19. Use the table in Ref. 36 to calculate f of Eq. II-25 for $r/V^{1/3}$ values of 0.40, 0.80, and 1.20.

20. Show how Eq. II-28 should be written if one includes the weight of liquid directly under the plate.

21. In a rotating drop measurement, what is the interfacial tension if the two liquids differ in density by 0.2 g/cm^3, the speed of rotation is 60 rpm, the volume of the drop is 0.4 cm^3, and the length of the extended drop is 6.5 cm?

22. For a particular drop of a certain liquid of density 0.83, β is -0.45 and d_e is 0.72 cm. (*a*) Calculate the surface tension of the drop and (*b*) calculate the drop profile from apex to the tip, assuming r_t/a to be 0.55, where r_t is the radius of the tip.

23. The surface tension of mercury is 471 dyn/cm at 24.5°C. In a series of measurements [37] the following drop weight data were obtained, (diameter of tip in centimeters, weight of drop in grams): (0.05167, 0.06407), (0.10068, 0.11535), (0.13027, 0.14245). Calculate the corresponding f and $r/V^{1/3}$ values.

24. Johnson and Lane [28] give the equation for the maximum bubble pressure:

$$h = \frac{a^2}{r} + \frac{2}{3}\frac{42}{r} + \frac{1}{6}\frac{r^3}{a^2}$$

For a certain liquid, $a^2 = 0.0780$ cm^2 and $r = 0.160$ cm. Calculate, using the equation, the values of X/r and r/a and compare with the X/r value given by Table II-2.

25. According to the simple formula, the maximum bubble pressure is given by $P_{max} = 2\gamma/r$ where r is the radius of the circular cross-section tube, and P has been corrected for the hydrostatic head due to the depth of immersion of the tube. Using the appropriate table, show what maximum radius tube may be used if γ computed by the simple formula is not to be more than 5% in error. Assume a liquid of $\gamma = 25$ dyn/cm and density 0.98 g/cm^3.

26. A liquid of density 2.0 g/cm^3 forms a meniscus of shape corresponding to $\beta = 80$ in a metal capillary tube with which the contact angle is 30°. The capillary rise is 0.063 cm. Calculate the surface tension of the liquid and the radius of the capillary, using Table II-1.

27. Equation II-30 may be integrated to obtain the profile of a meniscus against a vertical plate; the integrated form is given in Ref. 53. Calculate the meniscus profile for water at 20°C for (*a*) the case where water wets the plate and (*b*) the case where the contact angle is 40°. For (*b*) obtain from your plot the value of h, and compare with that calculated from Eq. II-28. [*Hint:* Obtain a^2 from II-15.]

28. An empirical observation is if one forms drops at a constant flow rate such that the drop time is t, then the observed drop mass, $M(t)$, varies with t according to the equation $M(t) = M_\infty + st^{-3/4}$ where M_∞ is the "equilibrium" value and s is a $9.44s + 5.37$. Using these two relationships, it is possible to determine surface tension as a

function of surface age by means of the drop weight method. Combine these equations to obtain one relating $M_\infty(t)$ and t, where $M_\infty(t)$ is the equilibrium drop mass (and the one to which Eq. II-25 applies) and surface age t. For a particular surfactant solution, the observed drop mass is 80.4 mg for drops formed very slowly and 125.7 mg for drops formed every 2 sec. The radius of the tip used is 5 mm and the density of the solution was 1.03 g/cm^3. Calculate the equilibrium surface tension and that for a surface age of 2 sec given (*a*) $f = 0.6456$; and (b) $f = 0.6043$. (Note Refs. 41 and 124.)

29. Estimate the surface tension of *n*-decane at 20°C using Eq. 11-39 and data in Table II-4.

General References

N. K. Adam, *The Physics and Chemistry of Surfaces*, 3rd ed., Oxford University Press, London, 1941.

R. Aveyard and D. A. Haydon, *An Introduction to the Principles of Surface Chemistry*, Cambridge University Press, Cambridge, UK, 1973.

J. T. Davies and E. K. Rideal, *Interfacial Phenomena*, 2nd ed., Academic, New York, 1963.

W. D. Harkins, *The Physical Chemistry of Surface Films*, Reinhold, New York, 1952.

P. C. Hiemenz, *Principles of Colloid and Surface Chemistry*, 2nd ed., Marcel Dekker, New York, 1986.

S. R. Morrison, *The Chemical Physics of Surfaces*, Plenum, London, 1977.

H. van Olphen and K. J. Mysels, *Physical Chemistry: Enriching Topics from Colloid and Surface Science*, Theorex (8327 La Jolla Scenic Drive), La Jolla, CA, 1975.

L. I. Osipow, *Surface Chemistry, Theory and Industrial Applications*, Krieger, New York, 1977.

J. S. Rowlinson and B. Widom, *Molecular Theory of Capillarity*, Clarendon Press, Oxford, 1984.

D. J. Shaw, *Introduction to Colloid and Surface Chemistry*, Butterworths, London, 1966.

Textual References

1. T. Young, in *Miscellaneous Works*, G. Peacock, ed., J. Murray, London, 1855, Vol. I, p. 418.
2. P. S. de Laplace, *Mechanique Celeste*, Supplement to Book 10, 1806.
3. C. V. Boys, *Soap Bubbles and the Forces that Mould Them*, Society for Promoting Christian Knowledge, London, 1890; reprint ed., Doubleday Anchor Books, Science Study Series S3, Doubleday, Garden City, NY, 1959.
4. F. D. Rumscheit and S. G. Mason, *J. Colloid Sci.*, **17,** 266 (1962).
5. D. H. Michael, *Ann. Rev. Fluid Mech.*, **13,** 189 (1981).
6. D. B. Bogy, *Ann. Rev. Fluid Mech.*, **11,** 207 (1979).

6a. A. Hajiloo, T. R. Ramamohan, and J. C. Slattery, *J. Colloid Interface Sci.*, **117,** 384 (1987).

7. See R. W. Coyle and J. C. Berg, *Chem. Eng. Sci.*, **39,** 168 (1984); H. C. Burkholder and J. C. Berg, *AIChE J.*, **20,** 863 (1974).
8. K. D. Bartle, C. L. Woolley, K. E. Markides, M. L. Lee, and R. S. Hansen, *J. High Resol. Chromatog. Chromatogr. Comm.*, **10,** 128 (1987).
9. R. Sen and W. R. Wilcox, *J. Crystal Growth*, **74,** 591 (1986).
10. E. Bayramli, A. Abou-Obeid, and T. G. M. Van de Ven, *J. Colloid Interface Sci.*, **116,** 490, 503 (1987).
11. E. A. Boucher, *Rep. Prog. Phys.*, **43,** 497 (1980).

11a. F. Morgan, *Am. Scient.*, **74,** 232 (1986).

12. H. M. Princen, in *Surface and Colloid Science*, E. Matijevic, ed., Vol. 2, Wiley-Interscience, New York, 1969.
13. Lord Rayleigh (J. W. Strutt), *Proc. Roy. Soc.* (London), **A92,** 184 (1915).
14. F. Bashforth and J. C. Adams, *An Attempt to Test the Theories of Capillary Action*, University Press, Cambridge, England, 1883.
15. S. Sugden, *J. Chem. Soc.*, **1921,** 1483.
16. J. E. Lane, *J. Colloid Interface Sci.*, **42,** 145 (1973).
17. J. F. Padday and A. Pitt, *J. Colloid Interface Sci.*, **38,** 323 (1972).
18. A. W. Adamson, *J. Chem. Ed.*, **55,** 634 (1978).
19. T. A. Erikson, *J. Phys. Chem.*, **69,** 1809 (1965).
20. T. W. Richards and E. K. Carver, *J. Am. Chem. Soc.*, **43,** 827 (1921).
21. W. D. Harkins and F. E. Brown, *J. Am. Chem. Soc.*, **41,** 499 (1919).
22. S. S. Urazovskii and P. M. Chetaev, *Kolloidn. Zh.*, **11,** 359 (1949); through *Chem. Abstr.*, **44,** 889 (1950).
23. P. R. Edwards, *J. Chem. Soc.*, **1925,** 744.
24. G. Jones and W. A. Ray, *J. Am. Chem. Soc.*, **59,** 187 (1937).
25. W. Heller, M. Cheng, and B. W. Greene, *J. Colloid Interface Sci.*, **22,** 179 (1966).
26. S. Ramakrishnan and S. Hartland, *J. Colloid Interface Sci.*, **80,** 497 (1981).
27. S. Sugden, *J. Chem. Soc.*, **1922,** 858; **1924,** 27.
28. C. H. J. Johnson and J. E. Lane, *J. Colloid Interface Sci.*, **47,** 117 (1974).
29. Y. Saito, H. Yoshida, T. Yokoyama, and Y. Ogina, *J. Colloid Interface Sci.*, **66,** 440 (1978).
30. S. Y. Park, C. H. Chang, D. J. Ahn, and E. I. Franses, *Langmuir*, **9,** 3640 (1993).
31. C. H. Chang and E. I. Franses, *Chem. Eng. Sci.*, **49,** 313 (1994).
32. R. Miller, A. Hofmann, R. Hartmann, K. H. Schano, and A. Halbig, *Adv. Materials*, **4,** 370 (1992).
33. T. Tate, *Phil. Mag.*, **27,** 176 (1864).
34. E. A. Boucher and M. J. B. Evans, *Proc. Roy. Soc.* (London), **A346,** 349 (1975).
35. E. A. Boucher and H. J. Kent, *J. Colloid Interface Sci.*, **67,** 10 (1978).
36. J. L. Lando and H. T. Oakley, *J. Colloid Interface Sci.*, **25,** 526 (1967).
37. M. C. Wilkinson and M. P. Aronson, *J. Chem. Soc., Faraday Trans. I,* **69,** 474 (1973).
38. R. Miller and K. H. Schano, *Tenside Surf. Det.*, **27,** 238 (1990).
39. R. Miller, K. H. Schano, and A. Hofmann, *Colloids & Surfaces*, **A92,** 189 (1994).

40. V. B. Fainerman and R. Miller, *Colloids & Surfaces*, **A97,** 255 (1995).
41. C. Jho and M. Carreras, *J. Colloid Interface Sci.*, **99,** 543 (1984).
42. P. Lecomte du Noüy, *J. Gen. Physiol.*, **1,** 521 (1919).
43. W. D. Harkins and H. F. Jordan, *J. Am. Chem. Soc.*, **52,** 1751 (1930).
44. C. Huh and S. G. Mason, *Colloid Polym. Sci.*, **253,** 566 (1975).
45. H. W. Fox and C. H. Chrisman, Jr., *J. Phys. Chem.*, **56,** 284 (1952).
46. A. G. Gaonkar and R. D. Neuman, *J. Colloid Interface Sci.*, **98,** 112 (1984).
47. J. A. Krynitsky and W. D. Garrett, *J. Colloid Sci.*, **18,** 893 (1963).
48. F. van Zeggeren, C. de Courval, and E. D. Goddard, *Can. J. Chem.*, **37,** 1937 (1959).
49. B. Maijgren and L. Ödberg, *J. Colloid Interface Sci.*, **88,** 197 (1982).
50. L. Wilhelmy, *Ann. Phys.*, **119,** 177 (1863).
51. D. O. Jordan and J. E. Lane, *Austral. J. Chem.*, **17,** 7 (1964).
52. J. T. Davies and E. K. Rideal, *Interfacial Phenomena*, Academic Press, New York, 1961.
53. A. W. Adamson and A. Zebib, *J. Phys. Chem.*, **84,** 2619 (1980).
54. A. W. Neumann and W. Tanner, *Tenside*, **4,** 220 (1967).
55. H. M. Princen, *Austral. J. Chem.*, **23,** 1789 (1970).
56. J. Kloubek and A. W. Neumann, *Tenside*, **6,** 4 (1969).
57. G. L. Gaines, Jr., *Insoluble Monolayers at Liquid-Gas Interfaces*, Interscience, New York, 1966; *J. Colloid Interface Sci.*, **62,** 191 (1977).
58. S. K. Li, R. P. Smith, and A. W. Neumann, *J. Adhesion*, **17,** 105 (1984).
59. R. A. Hayes, A. C. Robinson, and J. Ralston, *Langmuir*, **10,** 2850 (1994).
60. G. Loglio, U. Tesei, N. Delgi Innocenti, R. Miller, and R. Cini, *Colloids & Surfaces*, **57,** 335 (1991).
61. S. H. Anastasiadis, J. K. Chen, J. T. Koberstein, A. F. Siegel, J. E. Sohn, and J. A. Emerson, *J. Colloid Interface Sci.*, **119,** 55 (1987).
62. P. Cheng, D. Li, L. Boruvka, Y. Rotenberg, and A. W. Neumann, *Colloids & Surf.*, **43,** 151 (1990).
63. D. Li, P. Cheng, and A. W. Neumann, *Adv. Colloid & Interface Sci.*, **39,** 347 (1992).
64. S. Rooks, L. M. Racz, J. Szekely, B. Benhabib, and A. W. Neumann, *Langmuir*, **7,** 3222 (1991).
65. P. Cheng and A. W. Neumann, *Colloids & Surfaces*, **62,** 297 (1992).
66. J. M. Andreas, E. A. Hauser, and W. B. Tucker, *J. Phys. Chem.*, **42,** 1001 (1938).
67. D. O. Niederhauser and F. E. Bartell, *Report of Progress—Fundamental Research on the Occurrence and Recovery of Petroleum*, Publication of the American Petroleum Institute, The Lord Baltimore Press, Baltimore, 1950, p. 114.
68. S. Fordham, *Proc. Roy. Soc.* (London), **A194,** 1 (1948).
69. C. E. Stauffer, *J. Phys. Chem.*, **69,** 1933 (1965).
70. J. F. Boyce, S. Schürch, Y. Rotenburg, and A. W. Neumann, *Colloids & Surfaces*, **9,** 307 (1984).
71. Y. Rotenberg, L. Boruvka, and A. W. Neumann, *J. Colloid Interface Sci.*, **93,** 169 (1983).

72. S. H. Anastastadis, I. Gancarz, and J. T. Koberstein, *Macromolecules*, **21,** 2980 (1988).
73. C. Huh and R. L. Reed, *J. Colloid Interface Sci.*, **91,** 472 (1983).
74. H. H. J. Girault, D. J. Schiffrin, and B. D. V. Smith, *J. Colloid Interface Sci.*, **101,** 257 (1984).
75. D. Y. Kwok, D. Vollhardt, R. Miller, D. Li, and A. W. Neumann, *Colloids & Surfaces*, **A88,** 51 (1994).
76. J. Li, R. Miller, W. Wustneck, H. Mohwald, and A. W. Neumann, *Colloids & Surfaces*, **A96,** 295 (1995).
77. J. F. Padday, *Phil. Trans. Roy. Soc.* (London), **A269,** 265 (1971).
78. J. F. Padday, *Proc. Roy. Soc.* (London), **A330,** 561 (1972).
79. L. M. Coucoulas and R. A. Dawe, *J. Colloid Interface Sci.*, **103,** 230 (1985).
80. G. C. Nutting and F. A. Long, *J. Am. Chem. Soc.*, **63,** 84 (1941).
81. P. Kosakévitch, S. Chatel, and M. Sage, *CR*, **236,** 2064 (1953).
82. C. Kemball, *Trans. Faraday Soc.*, **42,** 526 (1946).
83. N. K. Roberts, *J. Chem. Soc.*, **1964,** 1907.
84. B. Widom, *J. Phys. Chem.*, **99,** 2803 (1995).
85. B. Vonnegut, *Rev. Sci. Inst.*, **13,** 6 (1942).
86. H. M. Princen, I. Y. Z. Zia, and S. G. Mason, *J. Colloid Interface Sci.*, *23,* 99 (1967).
87. J. C. Slattery and J. Chen, *J. Colloid Interface Sci.*, **64,** 371 (1978).
88. G. L. Gaines, Jr., *Polym. Eng.*, **12,** 1 (1972).
89. P. K. Currie and J. Van Nieuwkoop, *J. Colloid Interface Sci.*, **87,** 301 (1982).
90. J. L. Cayias, R. S. Schechter, and W. H. Wade, in *Adsorption at Interfaces*, K. L. Mittal, ed., ACS Symposium Series, **8,** 234 (1975); L. Cash, J. L. Cayias, G. Fournier, D. MacAllister, T. Schares, R. S. Schechter, and W. H. Wade, *J. Colloid Interface Sci.*, **59,** 39 (1977).
91. K. Shinoda and Y. Shibata, *Colloids & Surfaces*, **19,** 185 (1986).
92. J. Lucassen, *J. Colloid Interface Sci.*, **70,** 335 (1979).
93. J. M. Rallison, *Ann. Rev. Fluid Mech.*, **16,** 45 (1984).
93a. H. A. Stone, *Ann. Rev. Fluid Mech.*, **26,** 65 (1994).
94. C. T. O'Konski and P. L. Gunter, *J. Colloid Sci.*, **10,** 563 (1964).
95. S. Koriya, K. Adachi, and T. Kotaka, *Langmuir*, **2,** 155 (1986).
96. S. Torza, R. G. Cox, and S. G. Mason, *Phil. Trans. Roy. Soc.* (London), **269,** 295 (1971).
97. Lord Kelvin (W. Thomson), *Phil. Mag.*, **42,** 368 (1871).
98. A. Lawal and R. A. Brown, *J. Colloid Interface Sci.*, **89,** 332 (1982).
99. H. V. Nguyen, S. Padmanabhan, W. J. Desisto, and A. Bose, *J. Colloid Interface Sci.*, **115,** 410 (1987).
100. J. H. Bohorquez, B. P. Canfield, K. J. Courian, F. Drogo, C. A. E. Hall, C. L. Holstun, A. R. Scandalis, and M. E. Shepard, *Hewlett-Packard J.*, **45,** 9 (1994).
101. R. Miller, P. Joos, and V. B. Fainerman, *Adv. Colloid Interface Sci.*, **49,** 249 (1994).
102. C. H. Chang and E. I. Franses, *Colloids & Surfaces*, **A100,** 1 (1995).

103. K. L. Sutherland, *Austral. J. Chem.*, **7,** 319 (1954).
104. N. N. Kochurova and A. I. Rusanov, *J. Colloid Interface Sci.*, **81,** 297 (1981).
105. R. S. Hansen and T. C. Wallace, *J. Phys. Chem.*, **63,** 1085 (1959).
106. W. D. E. Thomas and D. J. Hall, *J. Colloid Interface Sci.*, **51,** 328 (1975).
107. D. A. Netzel, G. Hoch, and T. I. Marx, *J. Colloid Sci.*, **19,** 774 (1964).
108. R. S. Hansen, *J. Phys. Chem.*, **68,** 2012 (1964).
109. W. D. E. Thomas and L. Potter, *J. Colloid Interface Sci.*, **50,** 397 (1975).
110. C. C. Addison and T. A. Elliott, *J. Chem. Soc.*, **1949,** 2789.
111. F. H. Garner and P. Mina, *Trans. Faraday Soc.*, **55,** 1607 (1959).
112. J. Van Havenbergh and P. Joos, *J. Colloid Interface Sci.*, **95,** 172 (1983).
113. C. Hsu and R. E. Apfel, *J. Colloid Interface Sci.*, **107,** 467 (1985).
114. R. S. Hansen and J. Ahmad, *Progress in Surface and Membrane Science*, Vol. 4, Academic Press, New York, 1971.
115. H. Löfgren, R. D. Newman, L. E. Scriven, and H. T. Davis, *J. Colloid Interface Sci.*, **98,** 175 (1984).
116. S. Hård and R. D. Newman, *J. Colloid Interface Sci.*, **115,** 73 (1987).
117. M. Sano, M. Kawaguchi, Y-L. Chen, R. J. Skarlupka, T. Chang, G. Zographi, and H. Yu, *Rev. Sci. Instr.*, **57,** 1158 (1986).
118. J. C. Earnshaw and R. C. McGivern, *J. Phys. D: Appl. Phys.*, **20,** 82 (1987).
119. V. B. Fainerman, R. Miller, and P. Joos, *Colloid Polym. Sci.*, **272,** 731 (1994).
120. R. Miller, P. Joos, and V. B. Fainerman, *Prog. Colloid Polym. Sci.*, **97,** 188 (1994).
121. V. B. Fainerman, A. V. Makievski, and R. Miller, *Colloids & Surfaces*, **A75** (1993).
122. J. F. Padday and D. R. Russell, *J. Colloid Sci.*, **15,** 503 (1960).
123. D. G. LeGrand and G. L. Gaines, Jr., *J. Colloid Interface Sci.*, **42,** 181 (1973).
124. J. Kloubek, *Colloid Polymer Sci.*, **253,** 929 (1975).